

TRANSFORMER BLOCK COUPLING AND ITS CORRELATION WITH GENERALIZATION IN LLMs

Murdock Aubry* Haoming Meng* Anton Sugolov* Vardan Papyan

University of Toronto

ABSTRACT

Large Language Models (LLMs) have made significant strides in natural language processing, and a precise understanding of the internal mechanisms driving their success is essential. In this work, we trace the trajectories of individual tokens as they pass through transformer blocks, and linearize the system along these trajectories through their Jacobian matrices. By examining the relationships between these Jacobians, we uncover a **transformer block coupling** phenomenon in a variety of LLMs, characterized by the coupling of their top singular vectors across tokens and depth. Our findings reveal that coupling *positively correlates* with model performance, and that this relationship is stronger than with other hyperparameters, namely parameter budget, model depth, and embedding dimension. We further investigate the emergence of these properties through training, noting the development of coupling, as well as an increase in linearity and layer-wise exponential growth in the token trajectories. These collective insights provide a novel perspective on the interactions between token embeddings, and prompt further approaches to study training and generalization in LLMs.

1 INTRODUCTION

In recent years, many openly available Large Language Models (LLMs) have been released, achieving state-of-the-art results on task-specific benchmarks. The abundance of models, each with differing architecture and training methodology, motivates comparing the underlying mechanisms that drive generalization.

Transformers (Vaswani et al., 2017) can be represented as discrete, nonlinear, coupled dynamical systems, operating in high dimensions (Greff et al., 2016; Papyan et al., 2017; Haber & Ruthotto, 2017; Ee, 2017; Ebski et al., 2018; Chen et al., 2018; Bai et al., 2019; Rothauge et al., 2019; Gai & Zhang, 2021; Li & Papyan, 2023). The term *discrete* reflects the network’s finite depth; *nonlinear* refers to the model’s nonlinear components; *coupled* refers to the interdependent token trajectories enabled by self-attention, and *dynamical* is due to the residual connections spanning various layers.

Throughout this work, we investigate whether we can identify structural characteristics that consistently occur in pretrained LLMs that are related to their generalization, as measured on the Hugging-Face OpenLLM Leaderboard benchmark. To this end, we study and quantify the trajectories of token embeddings and their interactions, through linearizations of LLM layers given by the Jacobians of the associated transformer blocks.

This perspective raises several questions:

- Q1.** What regularity properties do these trajectories exhibit individually, and what are their relations with one another? More concretely, what is the relation between the Jacobians across different tokens and transformer layers?
- Q2.** How do the properties of hidden representations and their relations emerge with training?
- Q3.** Are any of these properties related to the generalization capabilities of LLMs?

*Equal contribution.

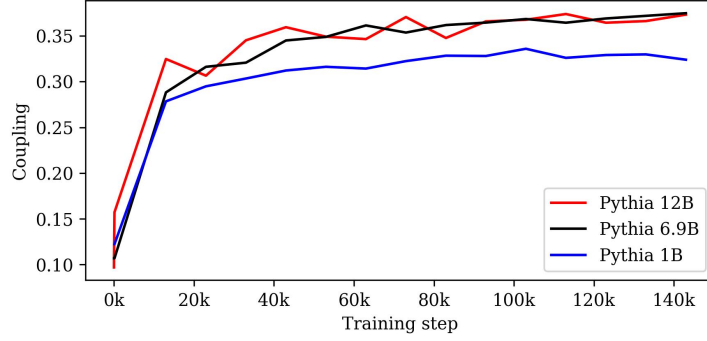


Figure 2: **Emergence of Singular Vector Coupling with Training.** Normalized coupling (Section 3.1) evaluated for $J_{i,j}^{d_1}, J_{i,j}^{d_2}$, with $|d_1 - d_2| \leq 5$. Measurements are taken for checkpoints of Pythia 12B, Pythia 6.9B, Pythia 1B (Biderman et al., 2023) at training steps $\{1, 16, 128, 13k, 23k, 33k, \dots, 143k\}$. Coupling is low at early training iterations, and increases with training, with Pythia 12B and 6.9B displaying greater coupling than Pythia 1B in final training steps.

nections:

$$h^{l+1}(X^l) = \text{MHA}(\text{LN}(X^l)) \quad (3)$$

$$g^{l+1}(X^l) = \text{LN}(X^l + h^{l+1}(X^l)) \quad (4)$$

$$f^{l+1}(X^l) = h^{l+1}(X^l) + \text{FFN}(g^{l+1}(X^l)) \quad (5)$$

$$F_{\text{block}}^{l+1}(X^l) = X^l + f^{l+1}(X^l), \quad (6)$$

where the MHA, LN, FFN are implicitly indexed by layer. Among many models (Appendix 1), an additional rotary positional embedding (RoPE, Su et al. (2023)) is applied in the MHA layer. In the final representation, typically an additional layer normalization is applied:

$$F_{\text{block}}^L(X^{L-1}) = \text{LN}(X^{L-1} + h^L(X^{L-1}) + \text{FFN}(g^L(X^{L-1}))). \quad (7)$$

The output X^L from the final block F^L is passed into a bias-free linear layer $M \in \mathbb{R}^{d_{\text{vocab}} \times d_{\text{model}}}$, with d_{vocab} denoting the size of the token vocabulary and d_{model} is the dimension of the token embeddings. This layer M computes final-layer logits for each token embedding, $\ell_i = Mx_i^L$. The prediction for the next token is then determined by selecting the maximal logit value: $\arg \max_{v \in \text{tokens}} \ell_{v,n}$.

3 METHODS

3.1 COUPLING OF SINGULAR VECTORS OF JACOBIANS

Jacobians. Coupling is investigated through analyzing the linearizations of transformer blocks given by their Jacobians

$$J_{t_1 t_2}^l = \frac{\partial}{\partial x_{t_1}^{l-1}} (f^l(X^{l-1}))_{t_2}, \quad (8)$$

defined for each layer $l \in \{1, \dots, L\}$, and pair of tokens $t_1, t_2 \in \{1, \dots, n\}$. Note that this is the Jacobian matrix for each transformer block without the contribution from the skip connection from the input of the block, similar to the quantity measured by Li & Papyan (2023), but extended for cross-token interactions. Also, due to the causal structure of the representations, $J_{t_1 t_2}^l = 0$ if $t_1 > t_2$, so we restrict our attention to the case $t_1 \leq t_2$.

Singular value decomposition. The SVD of the Jacobians $J_{t_1 t_2}^l$ are computed, i.e., $J_{t_1 t_2}^l = U_l S_l V_l^\top$ (with superscripts t_1, t_2 , indicating the tokens, omitted for clarity), where $U_l \in \mathbb{R}^{d_{\text{model}} \times d_{\text{model}}}$ and $V_l \in \mathbb{R}^{d_{\text{model}} \times d_{\text{model}}}$ are matrices of left and right singular vectors respectively, and $S_l \in \mathbb{R}^{d_{\text{model}} \times d_{\text{model}}}$ is the singular value matrix.

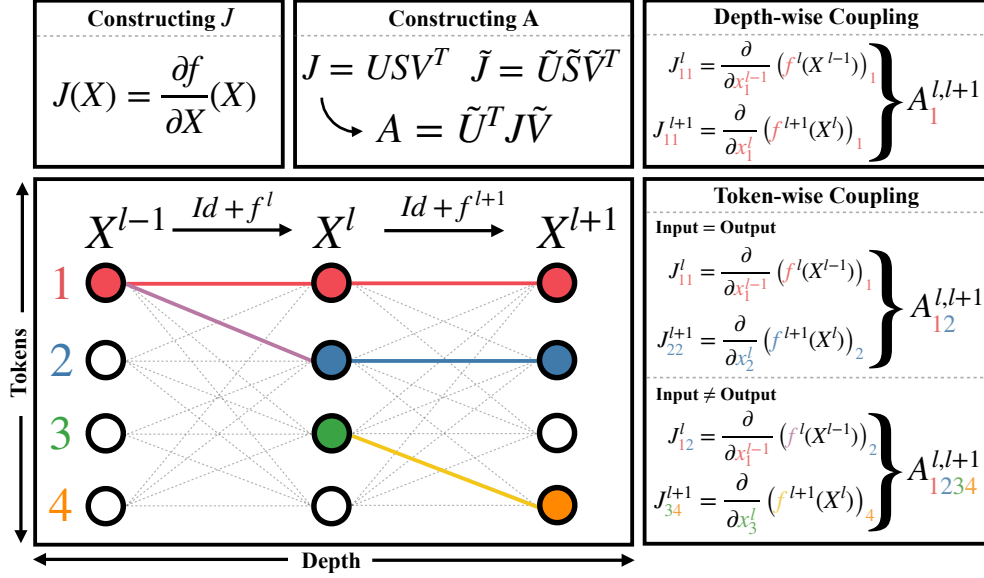


Figure 3: **Transformer Block Coupling.** Displayed is a visualization of the various types of transformer block coupling, along with brief instructions on computing both the Jacobians J and coupling matrices A .

To measure coupling between Jacobians $J_{t_1 t_2}^l$ and $J_{t'_1 t'_2}^{l'}$, define $A_{t_1 t_2 t'_1 t'_2}^{l',K} := U_{l',K}^\top J_{t_1 t_2}^l V_{l',K}$ for $l, l' \in \{1, \dots, L\}$ and $t_1, t_2, t'_1, t'_2 \in \{1, \dots, n\}$, where $U_{l',K}$ and $V_{l',K}$ are the sub-matrices with columns that are the top- K left and right singular vectors of $J_{t'_1 t'_2}^{l'}$, respectively.

Depth-wise Coupling. To analyze coupling across transformer blocks, we fix t (usually as the last token), and check alignment between J_{tt}^l and $J_{tt}^{l'}$ through $A_t^{l',K}$ (we write the single subscript t for clarity) across layers $l, l' \in \{1, \dots, L\}$.

Token-wise Coupling. To study the coupling across tokens, we start by fixing two layers $l, l' \in \{1, \dots, L\}$, and analyze coupling across different cases of the t_1, t_2, t'_1, t'_2 . We start with the case where the input and output tokens are the same and compare J_{tt}^l and $J_{t't'}^{l'}$ across $t, t' \in \{1, \dots, n\}$, which is the coupling across tokens for a token's effect on its own trajectory. We also consider the context tokens' impact on a trajectory by including coupling across cases with $t_1 < t_2$. More specifically, we measure coupling between $J_{t_1 t_2}^l$ and $J_{t'_1 t'_2}^{l'}$ across $t_2, t'_2 \geq t_1$ (fixing the input token to be the same) and also between $J_{t_1 t_2}^l$ and $J_{t'_1 t'_2}^{l'}$ across $t_1, t'_1 \leq t_2$ (fixing the output token to be the same).

Coupling measurement. To quantify the coupling of singular vectors of the Jacobians, we measure how far the $A_{t_1 t_2 t'_1 t'_2}^{l',K}$ are from being diagonal. More precisely, we quantify the mis-coupling of $A_{t_1 t_2 t'_1 t'_2}^{l',K}$ using $m : \mathbb{R}^{K \times K} \rightarrow \mathbb{R}$ defined by

$$m(A) = \|A - \text{Diag}(A)\|_F, \quad (9)$$

where $\text{Diag}(A)$ is the matrix A with all non-diagonal entries replaced by zero and $\|\cdot\|_F$ denotes the Frobenius norm. For normalized comparison between models across training in Figure 2, we normalize A by their norms

$$\tilde{m}(A) = \frac{\|A - \text{Diag}(A)\|_F}{\|A\|_F} \quad (10)$$

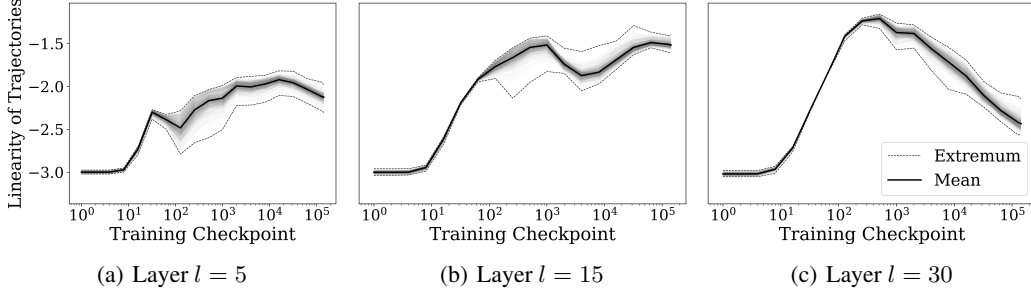


Figure 4: **Emergence of Linearity with Training.** Average linearity of a trajectory at block depths $l \in \{5, 15, 30\}$ evaluated for Pythia 12B (Biderman et al., 2023) checkpoints $\{1, 2, 4, \dots, 256, 512, 1k, 2k, 4k, \dots, 128k, 143k\}$. The linearity is given by the negative LSS, and is computed on a window of 11 layers centered at each depth l .

3.2 LINEARITY OF TRAJECTORIES

Linearity in intermediate embeddings is quantified with the *line-shape score* (LSS), defined by Gai & Zhang (2021) as

$$\text{LSS}_i^{0,\dots,L} = \frac{L}{\|\tilde{x}_i^L - \tilde{x}_i^0\|_2}, \quad (11)$$

where $\tilde{x}_i^0 = x_i^0$, i.e., the input embeddings passed to the LLM, and \tilde{x}_i^l is defined recursively as

$$\tilde{x}_i^l = \tilde{x}_i^{l-1} + \frac{x_i^l - x_i^{l-1}}{\|x_i^l - x_i^{l-1}\|_2} \text{ for } l = 1, \dots, L. \quad (12)$$

Note that $\text{LSS} \geq 1$, with $\text{LSS} = 1$ if and only if the intermediate representations x_i^0, \dots, x_i^L form a co-linear trajectory.

3.3 LAYER-WISE EXPONENTIAL GROWTH

We measure the presence of exponential spacing (*expodistance*) of the hidden trajectories. Assuming exponential growth of the embedding norms as they flow through the hidden layers, we can estimate,

$$\|x_i^l\| \approx e^{\alpha l} \|x_i^0\| = e^{\alpha} \|x_i^{l-1}\| \quad (13)$$

for some fixed $\alpha \in \mathbb{R}$ over all layers $l = 1, \dots, L$. We quantify the validity of the representation in Equation 13 by measuring the coefficient of variation of α_i^l , given by

$$\alpha_i^l \approx \ln \left(\frac{\|x_i^l\|}{\|x_i^{l-1}\|} \right), \quad (14)$$

for each layer l and token i . Under exponential growth, it is expected that α_i^l is independent of depth. We therefore denote the expodistance (ED) of the trajectory of the i^{th} token of a given sequence by

$$\text{ED}_i = \frac{\text{Var}_l \alpha_i^l}{(\text{Avg}_l \alpha_i^l)^2}. \quad (15)$$

This measurement is motivated by the parametrization discussed in Appendix A.4, as well as empirical evidence in Figure 22a, and serves as a method to test the validity of the linearization presented in Equation 17.

4 EVALUATION

4.1 SUITE OF LARGE LANGUAGE MODELS

Our study evaluates a total of 38 LLMs (24 base LLMs and 14 fine-tuned, see Appendix A.1) that were independently trained by various individuals and organizations. These models, provided

through HuggingFace (Wolf et al., 2020), vary in terms of parameter budgets, number of layers, hidden dimensions, and training tokens. Moreover, we analyze the dynamics of each measurement throughout training by deploying the Pythia Scaling Suite (Biderman et al., 2023). A summary of the models under consideration is presented in Table 1 of Appendix A.1 and further details in Appendix A.5.

4.2 PROMPT DATA

We evaluate these LLMs using prompts of varying length, ambiguity, and context, sourced from the test set of ARC (Clark et al., 2018), GSM8K (Cobbe et al., 2021), HellaSwag (Zellers et al., 2019), MMLU (Hendrycks et al., 2021), Truthful QA (Lin et al., 2022), and Winogrande (Sakaguchi et al., 2019). This data sets the performance benchmarks on the HuggingFace Open LLM Leaderboard (Beeching et al., 2023) and provide a representative evaluation of performance on many language tasks.

5 RESULTS

5.1 COUPLING OF JACOBIANS ACROSS DEPTH

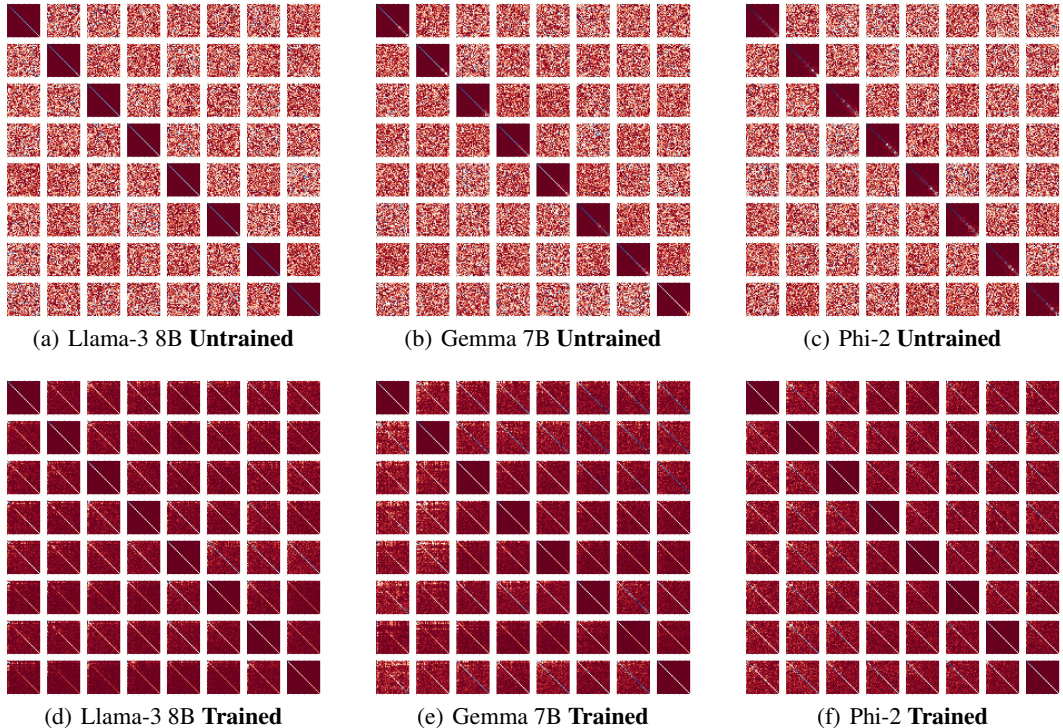


Figure 5: **Transformer Block Coupling across Depth.** The figure illustrates the coupling of Jacobians (across transformer blocks 9 to 16). In the matrix plot located at entry (l, l') , the absolute values of the entries of matrices $A_t^{ll',30}$ are visualized using the prompt 'What is the capital of France? The capital is', tracing the trajectory of its final token. The diagonal line in the trained plots (bottom row) with small off-diagonal entries indicates alignment of the Jacobians, where the top singular vectors of $J^{l'}$ diagonalize J^l . In the untrained models (top row), there is no alignment between singular vectors of Jacobians across layer. Additional visualizations are included in Appendix A.6 (Figure 13)

In trained LLMs, we observe coupling of the top singular vectors of the Jacobians across depth (Figure 5 bottom row), evident in the low non-diagonal values with a visible diagonal present in the matrix subplots. This is consistently observed across various LLMs considered. On the other hand,

in untrained models (Figure 5 top row), there is no coupling of Jacobians across different depths. There is coupling along the diagonal, however, because each Jacobian is trivially diagonalized by its own singular vectors. This, in addition to Figure 2, suggests that coupling across depth emerges through training.

5.2 COUPLING OF JACOBIANS ACROSS TOKENS

We also analyze the coupling of singular vectors of the Jacobians across tokens. First, we observe coupling between Jacobians where the input and output tokens are the same, that is, between J_l^{tt} and $J_{l'}^{t't'}$ across $t, t' \in \{1, \dots, n\}$ (Figure 6). This suggests that a token’s interaction on its own trajectory is coupled with that of other tokens. We also consider the context tokens’ interaction on a trajectory when fixing the input token t_1 (Figure 11), through $J_l^{t_1 t_2}$ and $J_{l'}^{t_1 t_2}$ across $t_2, t_2' \geq t_1$, and when fixing the output token t_2 (Figure 12), with $J_l^{t_1 t_2}$ and $J_{l'}^{t_1 t_2}$ across $t_1, t_1' \leq t_2$. Although generally present, the coupling in these two cases are less consistent, with variation in the strength of coupling between different token pairs. Again in untrained models (Figure 6 top row), there is a lack coupling of Jacobians across tokens.

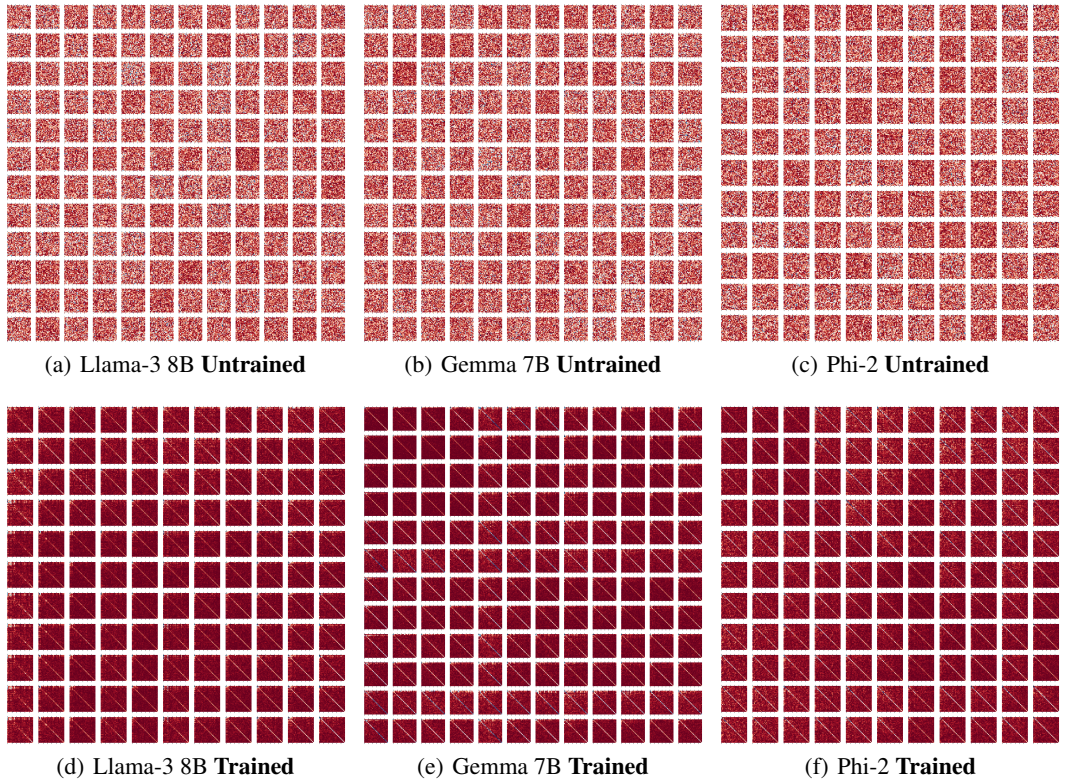


Figure 6: **Transformer Block Coupling across Tokens (Same input and output tokens)**. The figure illustrates coupling of Jacobians, with the same input and output token, across tokens. More specifically, in the matrix plot located at entry (t, t') , the absolute values of the entries of matrices $A_{ll'}^{ttt't'}$ are visualized (with randomly fixed layers l, l'). In the trained plots (bottom row), the off-diagonal entries being small with a visible diagonal indicates coupling of these Jacobians. At initialization (top row), there is no such coupling across tokens. Additional visualizations are included in Appendix A.6 (Figure 14).

5.3 EMERGENCE OF COUPLING WITH TRAINING

Coupling emerges through training for the evaluated LLMs, including coupling across depth (Figure 5) and across tokens (Figures 6, 11, 12). Further, we evaluate layer-wise coupling at intermediate

training checkpoints of Pythia 12B, 6.9B, and 1B (Biderman et al., 2023) (Figure 2), and observe that coupling is generally low at initialization and increases significantly during early training steps.

5.4 CORRELATION WITH GENERALIZATION

For each LLM, we measure the average coupling across depth (which we define to be negative mis-coupling) across prompts in the 6 evaluation datasets (Section 4.2), where for each prompt, $m(A_{ll',K}^n)$ is averaged over layers $l, l' \in \{1, \dots, L\}$. We plot the coupling values against the benchmark scores across several LLMs (Figure 1). Our results reveal a positive correlation between coupling and performance benchmark scores, and is more significant than the relationship between other significant model hyperparameters (Figure 25). This observation suggests a compelling relationship between stronger coupling of singular vectors of Jacobians $J_l^{t_1 t_2}$ and improved generalization.

5.5 REGULARITY IN HIDDEN TRAJECTORIES

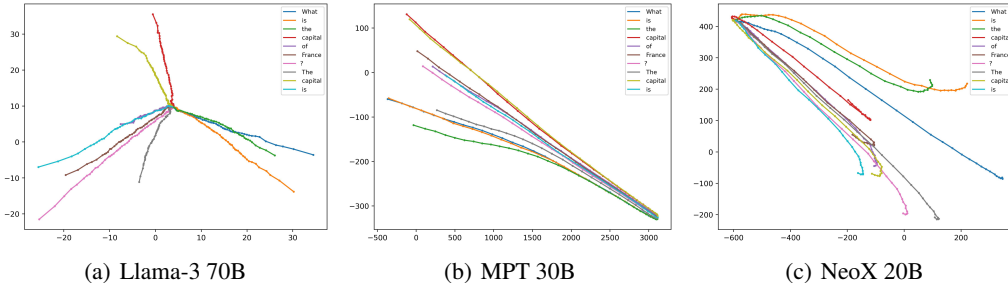


Figure 7: **Trajectories of Hidden Representations.** Visualization of the layer-wise trajectories of hidden representations in Llama 3 70B, Mistral 30B, and NeoX 20B in the prompt: What is the capital of France? The capital is. Trajectories of tokens are plotted in latent space, visualized with a 2-dimension principal component projection. A clear directed and outward growth is visible in each token trajectory.

We identify a considerable degree of linearity in the hidden trajectories of all featured LLMs. The LSS of the trajectories has an average value 4.25 in trained models, while taking average values of 6.54 at initialization, and is supported by the low variation across benchmark prompts (Figure 8). Linearity increases with training at varying depths of Pythia 12B (Figure 4). Linear and expansive behavior of the representations is demonstrated in Llama-3 70B, Mistral 30B, and NeoX 20B through low dimensional projections of embedding trajectories (Figure 7).

5.6 LAYER-WISE EXPONENTIAL GROWTH

Across all LLMs considered, the hidden trajectories exhibit exponential growth that emerges with training (Figure 9). The majority of the models exhibit a low coefficient of variation across prompts, showing the robustness of this property across a variety of tasks. The expodistance measurements show little dependence on model parameters, and take on consistently low values across all featured LLMs (Figure 9). In contrast, measurements at initialization show equally (rather than exponentially) distanced trajectories, as reflected by the low coefficients of variation in the norms of their layer-wise differences (Figure 18). Under certain assumptions, exponential spacing is justified in Section 6.2.

6 DISCUSSION

6.1 CORRELATION WITH GENERALIZATION

As discussed in Section 5.4, stronger coupling across Jacobian singular vectors is related to improved generalization (Figure 1). This relationship may assist in evaluating the training of transformers. In

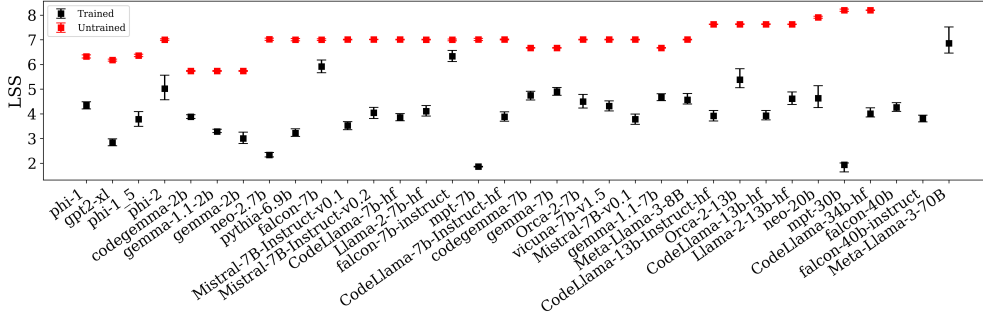


Figure 8: **Linearity of Trajectories.** The figure depicts the line-shape score (LSS) of embedding trajectories, as discussed in Section 5.5), computed on 1,200 prompts of the HuggingFace Open LLM Leaderboard (Section 4.2) for a variety of trained (black) and randomly initialized (red) LLMs (Appendix A.1). Plotted are the median values over all prompts, and are accompanied with uncertainty intervals depicting the inter-quartile range of the results for each model. Models are sorted by number of parameters.

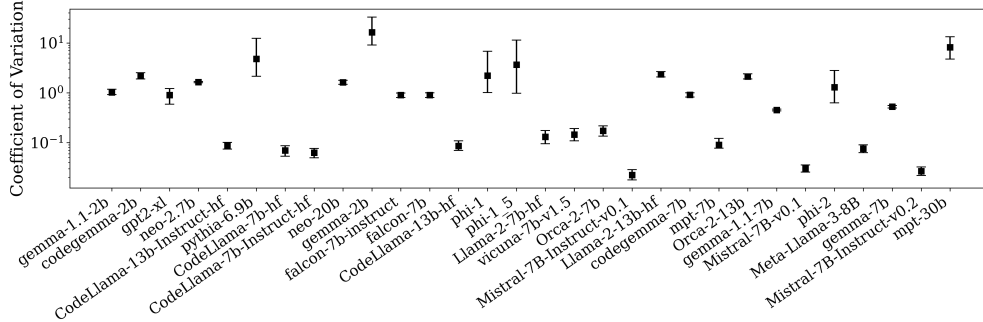


Figure 9: **Coefficient of variation of layer-wise exponent.** The figure presents the coefficient of variation of the layer-wise exponent (Section 3.3) computed on 1,200 prompts of the HuggingFace Open LLM Leaderboard (Section 4.2) for trained LLMs (Appendix A.1). Plotted are the median values over all prompts, and are accompanied with uncertainty intervals depicting the inter-quartile range of the results for each model. LLMs are sorted by increasing benchmark performance, while the vertical axis has a base 10 logarithmic scale.

particular, this finding suggests that the development of training methods to amplify coupling across transformer blocks may lead to favourable model performance.

6.2 EMERGENCE OF EXPONENTIAL SPACING WITH COUPLING

The emergence of exponential spacing in many LLMs can be viewed as a result of coupling under some assumptions on the homogeneity of the singular values across depth. Strong coupling suggests that the linearizations of hidden trajectories satisfy a linear difference equation (see Appendix A.4), given by

$$x^{l+1} - x^l = Ax^l$$

Considering the singular value decomposition of A in Equation 18 as $A = U\Sigma V^T$, and assuming that there is coupling ($U = V$), the difference equation can be diagonalized in the same basis across depth. Further assuming that the top singular values of the Jacobian blocks display low variation across depth, (Figure 24), we expect

$$\|x^l\| \approx e^{\sigma l} \|x^0\|, \tag{16}$$

where σ is the top singular value. Since we assume σ is independent of depth, the above norm is expected to be exponential in l , and offers an explanation to the measurements in Figure 9.

7 RELATED WORK

Residual Networks. ResNets (He et al., 2016) have been viewed as an ensemble of shallow networks (Veit et al., 2016), with studies delving into the scaling behaviour of their trained weights (Cohen et al., 2021). The linearization of residual blocks by their Residual Jacobians was first explored by Rothauge et al. (2019), who examined Residual Jacobians and their spectra in the context of stability analysis, and later by Li & Pappan (2023) who discovered Residual Alignment. Coupling of Jacobian singular vectors in LLM transformers extends previous results for classifier Resnets (Li & Pappan, 2023). We show coupling in $J_l^{t_1 t_2}$ across various tokens, which is specific to tokenization in transformers, in addition to demonstrating coupling of $J_l^{t_1 t_2}$ across l , which was also identified analogously in ResNets (Li & Pappan, 2023). Our measurements quantify the emergence with training of linearity and spacing, including at different depths, which was previously observed mostly qualitatively. Further comparison is included in Appendix A.3.

Neural ODE. Introduced by (Chen et al., 2018), Neural ODE view ResNets as a discretized dynamical process, with past work (Sander et al., 2022) showing the convergence of Residual Networks to a system of linear ODE. (Zhong et al., 2022; Li et al., 2021) studied neural ODE specific perspective to transformers and other LLM architectures. In our work, the presence of residual connections and emergence of Jacobian Alignment in transformers suggests that a discretization of a simple ODE emerges in LLMs.

Information Processing in LLMs. Previously, Katz & Belinkov (2023); Bietti et al. (2023) have described memory and semantic flow in intermediate states of transformers while van Aken et al. (2019) have examined BERT hidden trajectories. Investigation of LLMs for reasoning tasks and interpretability remains an important research focus (Huang & Chang, 2023).

In-context learning. Previous works have observed that LLMs are able to perform in context learning (von Oswald et al., 2023; Bai et al., 2024; Ahn et al., 2023; Akyürek et al., 2023; Xie et al., 2021; Hahn & Goyal, 2023; Xing et al., 2024): the model is capable of performing a particular machine learning task through a few examples provided in a single prompt or context. Their results consider a single layer of trained self-attention as implementing a single step of a gradient-descent-like learning rules across transformers depth, minimizing the MSE of a linear model

$$x_{\text{final}} = \min_x \|Ax - b\|^2$$

A gradient-descent learning rule would cause depth-wise updates to representations of the form

$$x_{t+1} = x_t + \epsilon A^T (Ax_t - b) = (I + \epsilon A^T A)x_t - \epsilon A^T b$$

We should expect similarity in the matrices $I + \epsilon A^T A$ across depth, which is suggested by coupling.

Hidden Representation Dynamics. Previous studies (Gai & Zhang, 2021; Haber & Ruthotto, 2017; Ee, 2017), have focused on interpreting deep neural networks from a dynamical systems perspective. Throughout training, numerical experiments have shown that both plain networks and ResNets are aptly approximated by a geodesic curve in Wasserstein space (Gai & Zhang, 2021). Other interpretations involve partitioning activation space into basins of attraction, with fixed points representing discrete thoughts (Nam et al., 2023). For further related works, see (Geshkovski et al., 2023b;a; Tarzanagh et al., 2023; Valeriani et al., 2023).

Structure in Hidden Representations. Emergence of regularity in last-layer representations during training was noticed in Neural Collapse (Pappan et al., 2020). Subsequent works examined structure of hidden representations and presented theoretical results describing the emergence of Neural Collapse (Wang et al., 2024a; Parker et al., 2023; Zangrando et al., 2024; Garrod & Keating, 2024; Wang et al., 2024b; Hoyt & Owen, 2021; Arous et al., 2023; Zarka et al., 2021; Ben-Shaul & Dekel, 2022; Pappan, 2020; Súkeník et al., 2023). Within LLMs, recent works have identified uniform structure in token means (Wu & Pappan, 2024), and low dimensional structure across hidden trajectories (Sarfati et al., 2024). Our work studies the representations of all layers in LLMs in a local sense through the interactions of tokens through their Jacobians.

8 LIMITATIONS

A limitation of the scope of our analysis is that due to the significant compute resources required to train LLMs of the size studied in this paper, our exploration is restricted to pretrained LLMs and

those fine-tuned on them. Several of these models are trained independently of each other, without carefully controlling for different experimental parameters. Consequently, direct comparisons between models become challenging, and so determining the cause of varying levels of regularity between LLMs becomes difficult. Nonetheless, this makes the consistent emergence of these properties interesting for further study.

9 CONCLUSION

Our primary goal was to contribute to the understanding of the mechanics underlying transformer architectures through an analysis of the trajectories of token embeddings and their interactions. Our research builds on the understanding of transformer architectures by revealing the coupling, across depth and token, of singular vectors in the Jacobians of transformer blocks for multiple LLMs trained by various organizations. We additionally observe and quantify the emergence of linearity and exponential spacing with training in the embedding trajectories of LLMs. Notably, we establish a correlation between the strength of this coupling and benchmark performance on the HuggingFace Open LLM Leaderboard, highlighting the significance of transformer block coupling for generalization. These findings open avenues for future research, encouraging deeper exploration into the connections between regularity of hidden representations, model specifications, and generalization.

REFERENCES

- Kwangjun Ahn, Xiang Cheng, Hadi Daneshmand, and Suvrit Sra. Transformers learn to implement preconditioned gradient descent for in-context learning, 2023.
- AI@Meta. Llama 3 model card. 2024. URL https://github.com/meta-llama/llama3/blob/main/MODEL_CARD.md.
- Ekin Akyürek, Dale Schuurmans, Jacob Andreas, Tengyu Ma, and Denny Zhou. What learning algorithm is in-context learning? investigations with linear models, 2023.
- Ebtesam Almazrouei, Hamza Alobeidli, Abdulaziz Alshamsi, Alessandro Cappelli, Ruxandra Cojocaru, Merouane Debbah, Etienne Goffinet, Daniel Heslow, Julien Launay, Quentin Malartic, Badreddine Noune, Baptiste Pannier, and Guilherme Penedo. Falcon-40B: an open large language model with state-of-the-art performance. 2023.
- Gerard Ben Arous, Reza Gheissari, Jiaoyang Huang, and Aukosh Jagannath. High-dimensional sgd aligns with emerging outlier eigenspaces, 2023.
- Shaojie Bai, J Zico Kolter, and Vladlen Koltun. Deep equilibrium models. *Advances in Neural Information Processing Systems*, 32, 2019.
- Yu Bai, Fan Chen, Huan Wang, Caiming Xiong, and Song Mei. Transformers as statisticians: Provable in-context learning with in-context algorithm selection. *Advances in neural information processing systems*, 36, 2024.
- Edward Beeching, Clémentine Fourier, Nathan Habib, Sheon Han, Nathan Lambert, Nazneen Rajani, Omar Sanseviero, Lewis Tunstall, and Thomas Wolf. Open llm leaderboard. https://huggingface.co/spaces/HuggingFaceH4/open_llm_leaderboard, 2023.
- Ido Ben-Shaul and Shai Dekel. Nearest class-center simplification through intermediate layers. In Alexander Cloninger, Timothy Doster, Tegan Emerson, Manohar Kaul, Ira Ktena, Henry Kvinge, Nina Miolane, Bastian Rieck, Sarah Tymochko, and Guy Wolf (eds.), *Proceedings of Topological, Algebraic, and Geometric Learning Workshops 2022*, volume 196 of *Proceedings of Machine Learning Research*, pp. 37–47. PMLR, 25 Feb–22 Jul 2022. URL <https://proceedings.mlr.press/v196/ben-shaul22a.html>.
- Stella Biderman, Hailey Schoelkopf, Quentin Anthony, Herbie Bradley, Kyle O’Brien, Eric Hallahan, Mohammad Aflah Khan, Shivanshu Purohit, USVSN Sai Prashanth, Edward Raff, Aviya Skowron, Lintang Sutawika, and Oskar van der Wal. Pythia: A suite for analyzing large language models across training and scaling, 2023.

- Alberto Bietti, Vivien Cabannes, Diane Bouchacourt, Herve Jegou, and Leon Bottou. Birth of a transformer: A memory viewpoint, 2023.
- Sid Black, Gao Leo, Phil Wang, Connor Leahy, and Stella Biderman. GPT-Neo: Large Scale Autoregressive Language Modeling with Mesh-Tensorflow, March 2021. URL <https://doi.org/10.5281/zenodo.5297715>. If you use this software, please cite it using these metadata.
- Sid Black, Stella Biderman, Eric Hallahan, Quentin Anthony, Leo Gao, Laurence Golding, Horace He, Connor Leahy, Kyle McDonell, Jason Phang, Michael Pieler, USVSN Sai Prashanth, Shivanshu Purohit, Laria Reynolds, Jonathan Tow, Ben Wang, and Samuel Weinbach. Gpt-neox-20b: An open-source autoregressive language model, 2022.
- Ricky TQ Chen, Yulia Rubanova, Jesse Bettencourt, and David K Duvenaud. Neural ordinary differential equations. *Advances in neural information processing systems*, 31, 2018.
- Peter Clark, Isaac Cowhey, Oren Etzioni, Tushar Khot, Ashish Sabharwal, Carissa Schoenick, and Oyvind Tafjord. Think you have solved question answering? try arc, the ai2 reasoning challenge, 2018.
- Karl Cobbe, Vineet Kosaraju, Mohammad Bavarian, Mark Chen, Heewoo Jun, Lukasz Kaiser, Matthias Plappert, Jerry Tworek, Jacob Hilton, Reiichiro Nakano, Christopher Hesse, and John Schulman. Training verifiers to solve math word problems, 2021.
- Alain-Sam Cohen, Rama Cont, Alain Rossier, and Renyuan Xu. Scaling properties of deep residual networks, 2021.
- Stanisław Jastrz Ebski, Devansh Arpit, Nicolas Ballas, Vikas Verma, Tong Che, and Yoshua Bengio. Residual connections encourage iterative inference. In *International Conference on Learning Representations*, 2018.
- Weinan Ee. A proposal on machine learning via dynamical systems. *Communications in Mathematics and Statistics*, 5:1–11, 02 2017. doi: 10.1007/s40304-017-0103-z.
- Kuo Gai and Shihua Zhang. A mathematical principle of deep learning: Learn the geodesic curve in the wasserstein space, 2021.
- Leo Gao, Stella Biderman, Sid Black, Laurence Golding, Travis Hoppe, Charles Foster, Jason Phang, Horace He, Anish Thite, Noa Nabeshima, et al. The pile: An 800gb dataset of diverse text for language modeling. *arXiv preprint arXiv:2101.00027*, 2020.
- Connell Garrod and Jonathan P. Keating. Unifying low dimensional observations in deep learning through the deep linear unconstrained feature model, 2024.
- Borjan Geshkovski, Cyril Letrouit, Yury Polyanskiy, and Philippe Rigollet. The emergence of clusters in self-attention dynamics. 2023a.
- Borjan Geshkovski, Cyril Letrouit, Yury Polyanskiy, and Philippe Rigollet. A mathematical perspective on transformers, 2023b.
- Klaus Greff, Rupesh K Srivastava, and Jürgen Schmidhuber. Highway and residual networks learn unrolled iterative estimation. *arXiv preprint arXiv:1612.07771*, 2016.
- Eldad Haber and Lars Ruthotto. Stable architectures for deep neural networks. *CoRR*, abs/1705.03341, 2017. URL <http://arxiv.org/abs/1705.03341>.
- Michael Hahn and Navin Goyal. A theory of emergent in-context learning as implicit structure induction. *arXiv preprint arXiv:2303.07971*, 2023.
- Kaiming He, Xiangyu Zhang, Shaoqing Ren, and Jian Sun. Deep residual learning for image recognition. In *2016 IEEE Conference on Computer Vision and Pattern Recognition (CVPR)*, pp. 770–778, 2016. doi: 10.1109/CVPR.2016.90.
- Dan Hendrycks, Collin Burns, Steven Basart, Andy Zou, Mantas Mazeika, Dawn Song, and Jacob Steinhardt. Measuring massive multitask language understanding, 2021.

- Christopher R. Hoyt and Art B. Owen. Probing neural networks with t-sne, class-specific projections and a guided tour, 2021.
- Jie Huang and Kevin Chen-Chuan Chang. Towards reasoning in large language models: A survey, 2023.
- Albert Q. Jiang, Alexandre Sablayrolles, Arthur Mensch, Chris Bamford, Devendra Singh Chaplot, Diego de las Casas, Florian Bressand, Gianna Lengyel, Guillaume Lample, Lucile Saulnier, L  lio Renard Lavaud, Marie-Anne Lachaux, Pierre Stock, Teven Le Scao, Thibaut Lavril, Thomas Wang, Timoth  e Lacroix, and William El Sayed. Mistral 7b, 2023.
- Shahar Katz and Yonatan Belinkov. Visit: Visualizing and interpreting the semantic information flow of transformers, 2023.
- Bei Li, Quan Du, Tao Zhou, Shuhan Zhou, Xin Zeng, Tong Xiao, and Jingbo Zhu. Ode transformer: An ordinary differential equation-inspired model for neural machine translation, 2021.
- Jianing Li and Vardan Papyan. Residual alignment: Uncovering the mechanisms of residual networks. In *Thirty-seventh Conference on Neural Information Processing Systems*, 2023.
- Stephanie Lin, Jacob Hilton, and Owain Evans. Truthfulqa: Measuring how models mimic human falsehoods, 2022.
- Andrew Nam, Eric Elmoznino, Nikolay Malkin, Chen Sun, Yoshua Bengio, and Guillaume Lajoie. Discrete, compositional, and symbolic representations through attractor dynamics, 2023.
- Vardan Papyan. Traces of class/cross-class structure pervade deep learning spectra, 2020.
- Vardan Papyan, Yaniv Romano, and Michael Elad. Convolutional neural networks analyzed via convolutional sparse coding. *The Journal of Machine Learning Research*, 18(1):2887–2938, 2017.
- Vardan Papyan, X. Y. Han, and David L. Donoho. Prevalence of neural collapse during the terminal phase of deep learning training. *Proceedings of the National Academy of Sciences*, 117(40):24652–24663, 2020. doi: 10.1073/pnas.2015509117. URL <https://www.pnas.org/doi/abs/10.1073/pnas.2015509117>.
- Liam Parker, Emre Onal, Anton Stengel, and Jake Intrater. Neural collapse in the intermediate hidden layers of classification neural networks, 2023.
- Alec Radford, Jeff Wu, Rewon Child, David Luan, Dario Amodei, and Ilya Sutskever. Language models are unsupervised multitask learners. 2019.
- Kai Rothauge, Zhewei Yao, Zixi Hu, and Michael W. Mahoney. Residual networks as nonlinear systems: Stability analysis using linearization, 2019.
- Baptiste Rozi  re, Jonas Gehring, Fabian Gloeckle, Sten Sootla, Itai Gat, Xiaoqing Ellen Tan, Yossi Adi, Jingyu Liu, Romain Sauvestre, Tal Remez, J  r  my Rapin, Artyom Kozhevnikov, Ivan Evtimov, Joanna Bitton, Manish Bhatt, Cristian Canton Ferrer, Aaron Grattafori, Wenhan Xiong, Alexandre D  fossez, Jade Copet, Faisal Azhar, Hugo Touvron, Louis Martin, Nicolas Usunier, Thomas Scialom, and Gabriel Synnaeve. Code llama: Open foundation models for code, 2024.
- Keisuke Sakaguchi, Ronan Le Bras, Chandra Bhagavatula, and Yejin Choi. WINOGRANDE: an adversarial winograd schema challenge at scale, 2019.
- Michael E. Sander, Pierre Ablin, and Gabriel Peyr  . Do residual neural networks discretize neural ordinary differential equations?, 2022.
- Rapha  l Sarfati, Toni J. B. Liu, Nicolas Boull  , and Christopher J. Earls. Lines of thought in large language models, 2024. URL <https://arxiv.org/abs/2410.01545>.
- Jianlin Su, Yu Lu, Shengfeng Pan, Ahmed Murtadha, Bo Wen, and Yunfeng Liu. Roformer: Enhanced transformer with rotary position embedding, 2023. URL <https://arxiv.org/abs/2104.09864>.

Peter SÚkeník, Marco Mondelli, and Christoph Lampert. Deep neural collapse is provably optimal for the deep unconstrained features model, 2023.

Davoud Ataee Tarzanagh, Yingcong Li, Xuechen Zhang, and Samet Oymak. Max-margin token selection in attention mechanism, 2023.

Gemma Team, Thomas Mesnard, Cassidy Hardin, Robert Dadashi, Surya Bhupatiraju, Shreya Pathak, Laurent Sifre, Morgane Rivière, Mihir Sanjay Kale, Juliette Love, Pouya Tafti, Léonard Hussenot, Pier Giuseppe Sessa, Aakanksha Chowdhery, Adam Roberts, Aditya Barua, Alex Botev, Alex Castro-Ros, Ambrose Slone, Amélie Héliou, Andrea Tacchetti, Anna Bulanova, Antonia Paterson, Beth Tsai, Bobak Shahriari, Charline Le Lan, Christopher A. Choquette-Choo, Clément Crepy, Daniel Cer, Daphne Ippolito, David Reid, Elena Buchatskaya, Eric Ni, Eric Noland, Geng Yan, George Tucker, George-Christian Muraru, Grigory Rozhdestvenskiy, Henryk Michalewski, Ian Tenney, Ivan Grishchenko, Jacob Austin, James Keeling, Jane Labanowski, Jean-Baptiste Lespiau, Jeff Stanway, Jenny Brennan, Jeremy Chen, Johan Ferret, Justin Chiu, Justin Mao-Jones, Katherine Lee, Kathy Yu, Katie Millican, Lars Lowe Sjoesund, Lisa Lee, Lucas Dixon, Machel Reid, Maciej Mikula, Mateo Wirth, Michael Sharman, Nikolai Chinaev, Nithum Thain, Olivier Bachem, Oscar Chang, Oscar Wahltinez, Paige Bailey, Paul Michel, Petko Yotov, Rahma Chaabouni, Ramona Comanescu, Reena Jana, Rohan Anil, Ross McIlroy, Ruibo Liu, Ryan Mullins, Samuel L Smith, Sebastian Borgeaud, Sertan Girgin, Sholto Douglas, Shree Pandya, Siamak Shakeri, Soham De, Ted Klimentko, Tom Hennigan, Vlad Feinberg, Wojciech Stokowiec, Yu hui Chen, Zafarali Ahmed, Zhitao Gong, Tris Warkentin, Ludovic Peran, Minh Giang, Clément Farabet, Oriol Vinyals, Jeff Dean, Koray Kavukcuoglu, Demis Hassabis, Zoubin Ghahramani, Douglas Eck, Joelle Barral, Fernando Pereira, Eli Collins, Armand Joulin, Noah Fiedel, Evan Senter, Alek Andreev, and Kathleen Kenealy. Gemma: Open models based on gemini research and technology, 2024.

MosaicML NLP Team. Introducing mpt-30b: Raising the bar for open-source foundation models, 2023a. URL www.mosaicml.com/blog/mpt-30b. Accessed: 2023-06-22.

MosaicML NLP Team. Introducing mpt-7b: A new standard for open-source, commercially usable llms, 2023b. URL www.mosaicml.com/blog/mpt-7b. Accessed: 2023-05-05.

Hugo Touvron, Louis Martin, Kevin Stone, Peter Albert, Amjad Almahairi, Yasmine Babaei, Nikolay Bashlykov, Soumya Batra, Prajjwal Bhargava, Shruti Bhosale, Dan Bikel, Lukas Blecher, Cristian Canton Ferrer, Moya Chen, Guillem Cucurull, David Esiobu, Jude Fernandes, Jeremy Fu, Wenyin Fu, Brian Fuller, Cynthia Gao, Vedanuj Goswami, Naman Goyal, Anthony Hartshorn, Saghar Hosseini, Rui Hou, Hakan Inan, Marcin Kardas, Viktor Kerkez, Madian Khabsa, Isabel Kloumann, Artem Korenev, Punit Singh Koura, Marie-Anne Lachaux, Thibaut Lavril, Jenya Lee, Diana Liskovich, Yinghai Lu, Yuning Mao, Xavier Martinet, Todor Mihaylov, Pushkar Mishra, Igor Molybog, Yixin Nie, Andrew Poulton, Jeremy Reizenstein, Rashi Rungta, Kalyan Saladi, Alan Schelten, Ruan Silva, Eric Michael Smith, Ranjan Subramanian, Xiaoqing Ellen Tan, Binh Tang, Ross Taylor, Adina Williams, Jian Xiang Kuan, Puxin Xu, Zheng Yan, Iliyan Zarov, Yuchen Zhang, Angela Fan, Melanie Kambadur, Sharan Narang, Aurelien Rodriguez, Robert Stojnic, Sergey Edunov, and Thomas Scialom. Llama 2: Open foundation and fine-tuned chat models, 2023.

Lucrezia Valeriani, Diego Doimo, Francesca Cuturello, Alessandro Laio, Alessio Ansuini, and Alberto Cazzaniga. The geometry of hidden representations of large transformer models, 2023.

Betty van Aken, Benjamin Winter, Alexander Löser, and Felix A. Gers. How does bert answer questions? a layer-wise analysis of transformer representations. In *Proceedings of the 28th ACM International Conference on Information and Knowledge Management, CIKM '19*, pp. 1823–1832, New York, NY, USA, 2019. Association for Computing Machinery. ISBN 9781450369763. doi: 10.1145/3357384.3358028. URL <https://doi.org/10.1145/3357384.3358028>.

Ashish Vaswani, Noam Shazeer, Niki Parmar, Jakob Uszkoreit, Llion Jones, Aidan N Gomez, Łukasz Kaiser, and Illia Polosukhin. Attention is all you need. 30, 2017. URL https://proceedings.neurips.cc/paper_files/paper/2017/file/3f5ee243547dee91fbd053c1c4a845aa-Paper.pdf.

- Andreas Veit, Michael Wilber, and Serge Belongie. Residual networks behave like ensembles of relatively shallow networks, 2016.
- Johannes von Oswald, Eyvind Niklasson, Ettore Randazzo, João Sacramento, Alexander Mordvintsev, Andrey Zhmoginov, and Max Vladymyrov. Transformers learn in-context by gradient descent, 2023.
- Peng Wang, Xiao Li, Can Yaras, Zihui Zhu, Laura Balzano, Wei Hu, and Qing Qu. Understanding deep representation learning via layerwise feature compression and discrimination, 2024a.
- Sicong Wang, Kuo Gai, and Shihua Zhang. Progressive feedforward collapse of resnet training, 2024b.
- Thomas Wolf, Lysandre Debut, Victor Sanh, Julien Chaumond, Clement Delangue, Anthony Moi, Pierric Cistac, Tim Rault, Rémi Louf, Morgan Funtowicz, Joe Davison, Sam Shleifer, Patrick von Platen, Clara Ma, Yacine Jernite, Julien Plu, Canwen Xu, Teven Le Scao, Sylvain Gugger, Mariama Drame, Quentin Lhoest, and Alexander M. Rush. Huggingface’s transformers: State-of-the-art natural language processing, 2020.
- Robert Wu and Vardan Papyan. Linguistic collapse: Neural collapse in (large) language models, 2024. URL <https://arxiv.org/abs/2405.17767>.
- Sang Michael Xie, Aditi Raghunathan, Percy Liang, and Tengyu Ma. An explanation of in-context learning as implicit bayesian inference. *arXiv preprint arXiv:2111.02080*, 2021.
- Yue Xing, Xiaofeng Lin, Namjoon Suh, Qifan Song, and Guang Cheng. Benefits of transformer: In-context learning in linear regression tasks with unstructured data. *arXiv preprint arXiv:2402.00743*, 2024.
- Emanuele Zangrando, Piero Deidda, Simone Brugiapaglia, Nicola Guglielmi, and Francesco Tudisco. Neural rank collapse: Weight decay and small within-class variability yield low-rank bias, 2024.
- John Zarka, Florentin Guth, and Stéphane Mallat. Separation and concentration in deep networks, 2021.
- Rowan Zellers, Ari Holtzman, Yonatan Bisk, Ali Farhadi, and Yejin Choi. Hellaswag: Can a machine really finish your sentence?, 2019.
- Yaofeng Desmond Zhong, Tongtao Zhang, Amit Chakraborty, and Biswadip Dey. A neural ode interpretation of transformer layers, 2022.

A APPENDIX AND SUPPLEMENTARY MATERIAL

A.1 SUITE OF LARGE LANGUAGE MODELS AND PROMPT DATA

We evaluate 38 total LLMs (24 base LLMs and 14 fine-tuned) on 6 datasets from the HuggingFace Open LLM leaderboard (Beeching et al., 2023).

Base models. Falcon (40B, 7B) (Almazrouei et al., 2023), Llama-3 (70B, 8B) (AI@Meta, 2024), Llama-2 (70B, 13B, 7B) (Touvron et al., 2023), MPT (30B, 7B) (Team, 2023a;b), Mistral v0.1 (Jiang et al., 2023), Gemma (7B, 2B) (Team et al., 2024), Gemma 1.1 (7B, 2B), NeoX (20B) (Black et al., 2022), Neo (2.7B) (Black et al., 2021; Gao et al., 2020), Pythia (6.9B). (Biderman et al., 2023), and GPT-2 (1.5B, 774M, 355M, 117M) (Radford et al., 2019).

Fine-tuned models. CodeLlama (34B, 13B, 7B) (Rozière et al., 2024), CodeLlama Instruct (34B, 13B, 7B) (Rozière et al., 2024), Mistral-v0.1 Instruct (7.3B) (Jiang et al., 2023), Mistral-v0.2 Instruct (Jiang et al., 2023), CodeGemma (Team et al., 2024).

Datasets. ARC (Clark et al., 2018), HellaSwag (Zellers et al., 2019), MMLU (Hendrycks et al., 2021), Truthful QA (Lin et al., 2022), WinoGrande (Sakaguchi et al., 2019).

Table 1: **LLMs featured in the experiments throughout paper.** Included in the table is the parameter budget of each model, the embedding dimension, the number of training tokens, and the Open LLM leaderboard (Beeching et al., 2023) benchmark score.

MODEL	PARAM.	LAYERS (L)	DIM. (d_{MODEL})	TOKENS	SCORE	POS.ENCODING
LLAMA-3	70 B	80	8192	15 T		RoPE
	8 B	32	4096	15 T	62.35	RoPE
LLAMA-2	70 B	80	8192	2 T	66.05	RoPE
	13 B	40	5120	2 T	55.69	RoPE
	7 B	32	4096	2 T	50.97	RoPE
CODELLAMA	34 B	48	8192	2 T	55.33	RoPE
	13 B	40	5120	2 T	45.82	RoPE
	7 B	32	4096	2 T	39.81	RoPE
CODELLAMA (IT)	34 B	48	8192	2 T	43.0	RoPE
	13 B	40	5120	2 T	37.52	RoPE
	7 B	32	4096	2 T	40.05	RoPE
ORCA	13 B	40	5120	2 T	58.64	RoPE
	7 B	32	4096	2 T	54.55	RoPE
FALCON	40 B	60	8192	1 T	58.07	RoPE
	7 B	32	4544	1.5 T	44.17	RoPE
FALCON (IT)	40 B	60	8192	1 T	43.26	RoPE
	7 B	32	4544	1.5 T		RoPE
MPT	30 B	48	7168	1 T	66.98	ALiBi
	7 B	32	4096	1 T	56.83	ALiBi
PHI	2 B	32	2560	1.4 T	61.33	RoPE
	1.5 B	24	2048	150 B	47.69	RoPE
	1 B	24	2048	54 B		RoPE
MISTRAL-V0.1	7.3 B	32	4096		60.97	ALiBi
MISTRAL-V0.1 (IT)	7.3 B	32	4096		54.96	ALiBi
MISTRAL-V0.2 (IT)	7.3 B	32	4096		65.71	ALiBi
GEMMA	7 B	28	3072	6 T	64.29	RoPE
	2 B	18	2048	6 T	42.75	RoPE
GEMMA-1.1	7 B	28	3072	6 T	30.0	RoPE
	2 B	18	2048	6 T	60.09	RoPE
CODEGEMMA	7 B	28	3072	6 T	56.73	RoPE
	2 B	18	2048	6 T	32.19	RoPE
NEO	20 B	44	6144		41.69	RoPE
	2.7 B	32	2560	0.42	36.20	SINE
PYTHIA	12 B	36	5120	0.3 T	58.9	RoPE
	6.9 B	32	4096	0.3 T	39.30	RoPE
	2.8 B	32	2560	0.3 T		RoPE
	1.4 B	24	2048	0.3 T		RoPE
	1 B	16	2048	0.3 T		RoPE
GPT-2	1.5 B	48	1600		34.12	SINE
	774 M	36	1280		32.07	SINE
	355 M	24	1024		29.87	SINE
	117 M	12	768		28.53	SINE

A.2 ADDITIONAL METRICS

A.2.1 VISUALIZATION OF TRAJECTORIES WITH PCA

Each token, with initial embedding x_i^0 , forms a trajectory $x_i^0, x_i^1, \dots, x_i^L$ as it passes through the L transformer blocks. The dynamics in high-dimensional space are visualized through a 2-dimensional principal component (PC) projection, PC_L , fitted to the last layer embeddings $X^L = (x_1^L, x_2^L, \dots, x_n^L)$. The projected embeddings, $\text{PC}_L(x_i^0), \text{PC}_L(x_i^1), \dots, \text{PC}_L(x_i^L)$, are plotted for each of the $i = 1, \dots, n$ trajectories.

A.3 COMPARISON TO RESNETS

Coupling. Our results complement and build upon those of (Li & Pappayan, 2023), who have observed the coupling of singular vectors of Residual Jacobians in classification ResNets. We

observe coupling across depth in a wide range of LLMs, where Jacobians are evaluated at the sequence of embeddings, with respect to the current token, whereas in RA Jacobians are evaluated at a single representation. Additionally, with transformers we may analyze coupling not only across depth but also across tokens. We observe coupling in LLMs across tokens in a variety of ways. Further, we consider and analyze the relationship between coupling and generalization.

Linearity and Equidistance. Linearity in hidden trajectories, as observed in ResNets Li & Pappan (2023); Gai & Zhang (2021), also emerges with training in LLMs. The mean LSS value among the evaluated LLMs is 4.24 (Figure 8), greater than LSS measurements observed for ResNets (Gai & Zhang (2021), page 18) which range between 2.0-3.0 (due to varying trajectory length and hidden dimension). In both architectures, training induces improved linearity and regularity (Figure 7) in trajectories. In contrast to ResNets, trajectories are not equidistant, instead showing exponential growth between layers (Figure 9). We quantify this spacing through a low coefficient of variation, displaying the presence of exponential growth in token trajectories. In both classifier ResNets and LLM transformers, there is an evident level of regularity in hidden representations (Figure 7).

Rank of Jacobians. Li & Pappan (2023) show that residual Jacobians have rank at most C , the number of classes. This analogous result automatically holds for LLMs since the vocabulary size is significantly greater than the embedding dimension of the transformer blocks.

Singular Value Scaling. Li & Pappan (2023) observe that top singular values of residual Jacobians scale inversely with depth. In trained LLMs, however, top singular values do not show a consistent depth scaling across models (Figure 24), notably differing from classification ResNets. In addition, the distribution of singular values at each layer varies significantly between models. Singular value scaling is more present in untrained transformers (Figure 23), likely caused by additional layer normalizations in residual blocks (Section 4.1).

A.4 DYNAMICAL MOTIVATION

The equality of top left and right singular vectors suggests that the linearizations form a simple dynamical system that acts on representations. Consider a homogenous linear ODE:

$$x' = Ax \tag{17}$$

Its solution is given by

$$x(t) = \exp(tA)x(0) = \lim_{L \rightarrow \infty} \left(I + \frac{At}{L} \right)^L x(0) \tag{18}$$

where the product is repeated L times. Expanding the brackets shows that $x(t)$ can be thought of as a collection of many paths of various lengths, due to the binomial identity. This agrees with Veit et al. (2016) which views ResNets as

$$x(t) = \left(I + \frac{tA_1}{L} \right) \left(I + \frac{tA_2}{L} \right) \dots \left(I + \frac{tA_L}{L} \right) x(0) \tag{19}$$

However, Veit et al. (2016) do not make any assumptions about the alignment of the various A_i matrices. The coupling phenomenon suggests ResNets as implementing the simpler system

$$x(t) = \left(I + \frac{tA}{L} \right) \left(I + \frac{tA}{L} \right) \dots \left(I + \frac{tA}{L} \right) x(0), \tag{20}$$

where all the A_i matrices are aligned. One benefit of this interpretation is that, as $L \rightarrow \infty$, we can write $x(t)$ in a simple closed form, namely $x(t) = \exp(tA)x(0)$.

Borrowing from the dynamical perspective, we quantify the similarity of hidden trajectories to the evolution of a linear ODE, in order to detect the emergence of a simple linearization to representations.

A.5 EXPERIMENTAL AND IMPLEMENTATION DETAILS

The source code used to produce the results reported in this experiment has been included as supplemental material. Models with varying parameter sizes are loaded on GPUs with appropriate memory

requirements: NVIDIA A40 ($n_{\text{param}} \geq 40B$), NVIDIA Quadro RTX 6000 for Gemma variants and when ($40B > n_{\text{param}} > 13B$), and NVIDIA Tesla T4 when ($13B \geq n_{\text{param}}$) except Gemma variants. 1,200 prompts from the OpenLLM leaderboard were evaluated in variable batch sizes were queued on a SLURM cluster, with appropriate adjustments depending on the memory required to load the LLM.

- $13B \geq n_{\text{param}}$: 100 prompts per batch, except Gemma variants, which used 25 prompts per batch. The larger memory requirement for Gemma variants is likely due to the much larger vocabulary size in the model.
- $40B > n_{\text{param}} > 13B$: 10 prompts per batch, except NeoX 20B which used 100 prompts per batch.
- $n_{\text{param}} \geq 40B$: 50 prompts per batch.

Due to the high memory requirement for computing Jacobians, for experiments involving the Jacobians, NVIDIA Quadro RTX 6000 was used additionally for $13B > n_{\text{param}} \geq 7B$ and corresponding models were quantized. Additionally, due to compute restrictions, alignment of singular vectors of Jacobians was computed on a smaller subset of the 1,200 prompts.

A.6 ADDITIONAL EXPERIMENTAL RESULTS

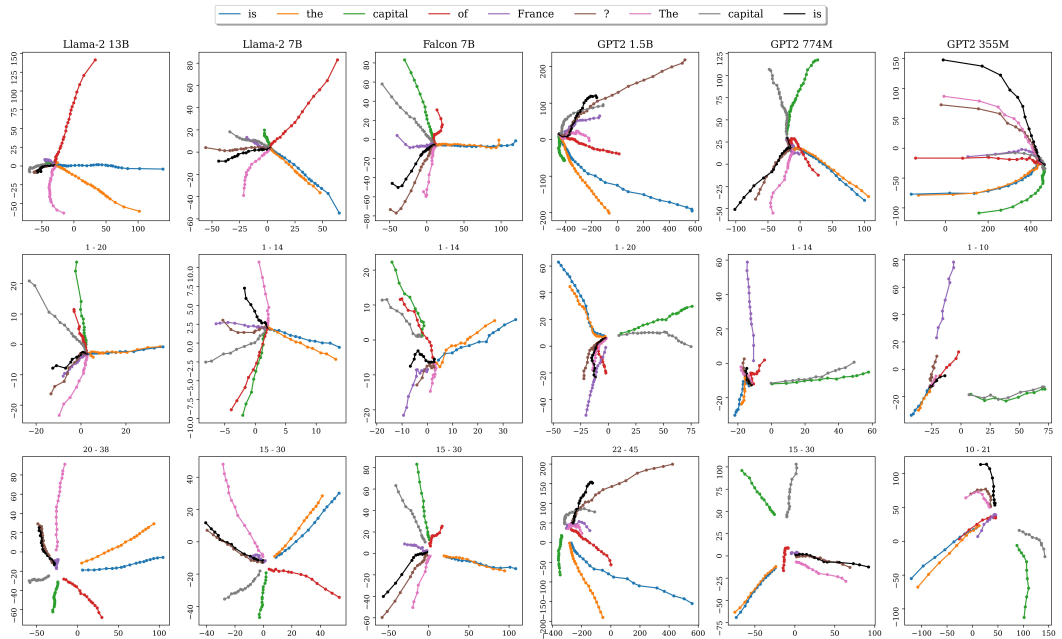


Figure 10: **Hidden Trajectories in LLMs.** Principal components of the trajectories of the hidden representations through various LLMs (columns, decreasing in model size, see Table 1) in the prompt: What is the capital of France? The capital is. Top row: all layers. Middle Row: layers in shallower transformer blocks (layers specified above plot). Bottom Row: layers in deeper transformer blocks (layers specified above plot). Trajectories of each input token (last token ‘is’ is plotted in black) are plotted in latent space, visualized with a 2-dimension principal component projection. Representations proceed in distinct outward directions, especially in the second half of transformer blocks (lower row) during which the norm of representations increases, with possible abrupt change in the last layer (outer points in upper row). A clear direction of movement is visible in each token trajectory.

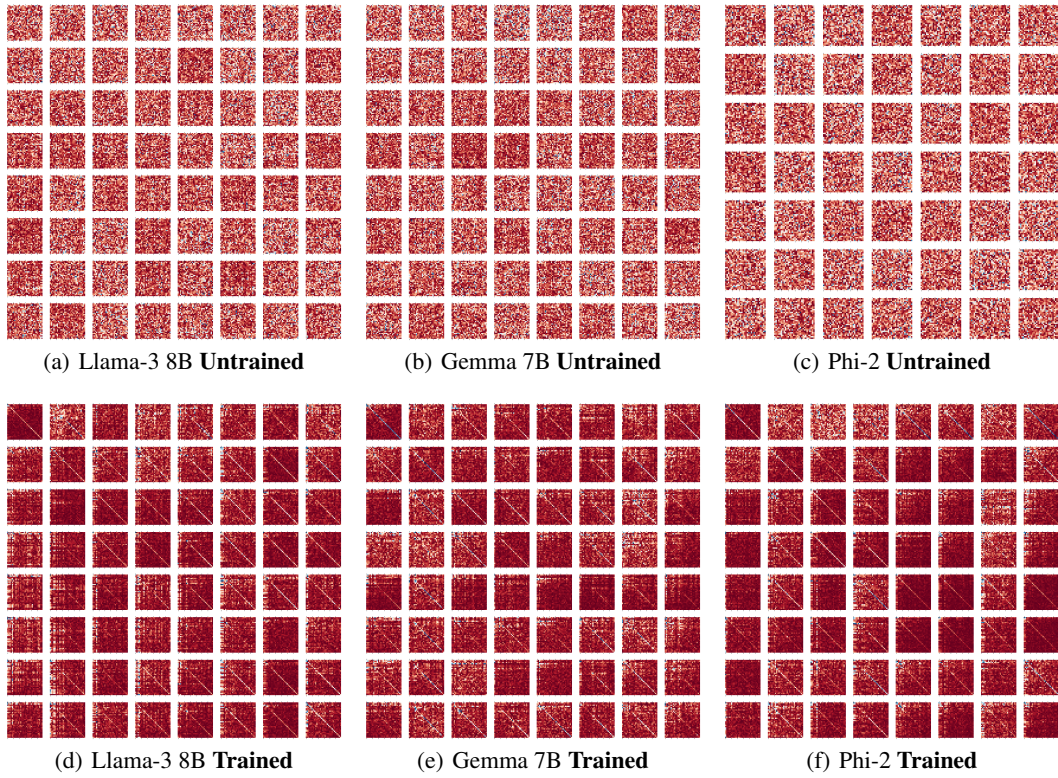


Figure 11: **Transformer Block Coupling across Token (Fixed input)**. The figure illustrates coupling of Jacobians, with fixed input token, across tokens. More specifically, in the matrix plot located at entry (t_2, t'_2) , the absolute values of the entries of matrices $A_{l'}^{t_1 t_2 t_1 t'_2}$ are visualized (with randomly fixed layers l, l'). In the trained plots (bottom row), the off-diagonal entries being close to 0 with visible diagonal indicates coupling of these Jacobians. This coupling, however, seems to be more evident for certain token pairs and less for others. At initialization (top row), there is no such coupling across tokens. Additional visualizations are included in Appendix A.6 (Figure 15)

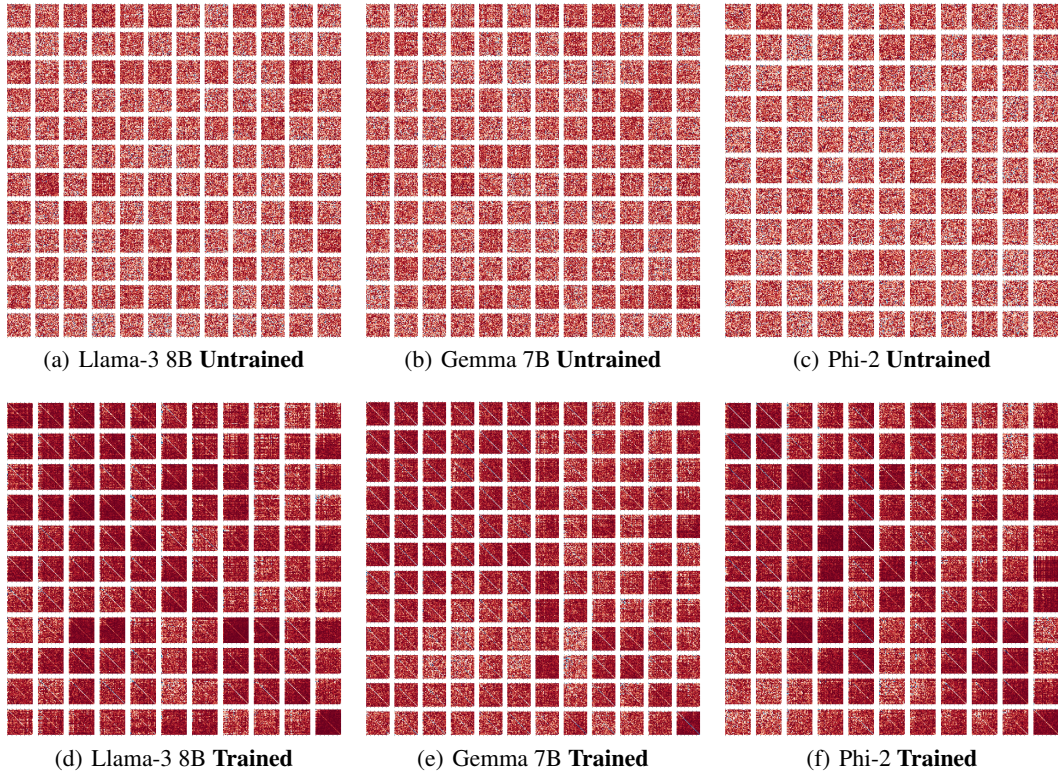


Figure 12: **Transformer Block Coupling across Token (Fixed output)**. The figure illustrates coupling of Jacobians, with fixed output token, across tokens. More specifically, in the matrix plot located at entry (t_1, t'_1) , the absolute values of the entries of matrices $A_{l'}^{t_1 t_2 t'_1 t_2}$ are visualized (with randomly fixed layers l, l'). In the trained plots (bottom row), the off-diagonal entries being close to 0 with visible diagonal indicates coupling of these Jacobians. This coupling again seems to be more evident only for certain token pairs. At initialization (top row), there is no such coupling across tokens. Additional visualizations are included in Appendix A.6 (Figure 16)

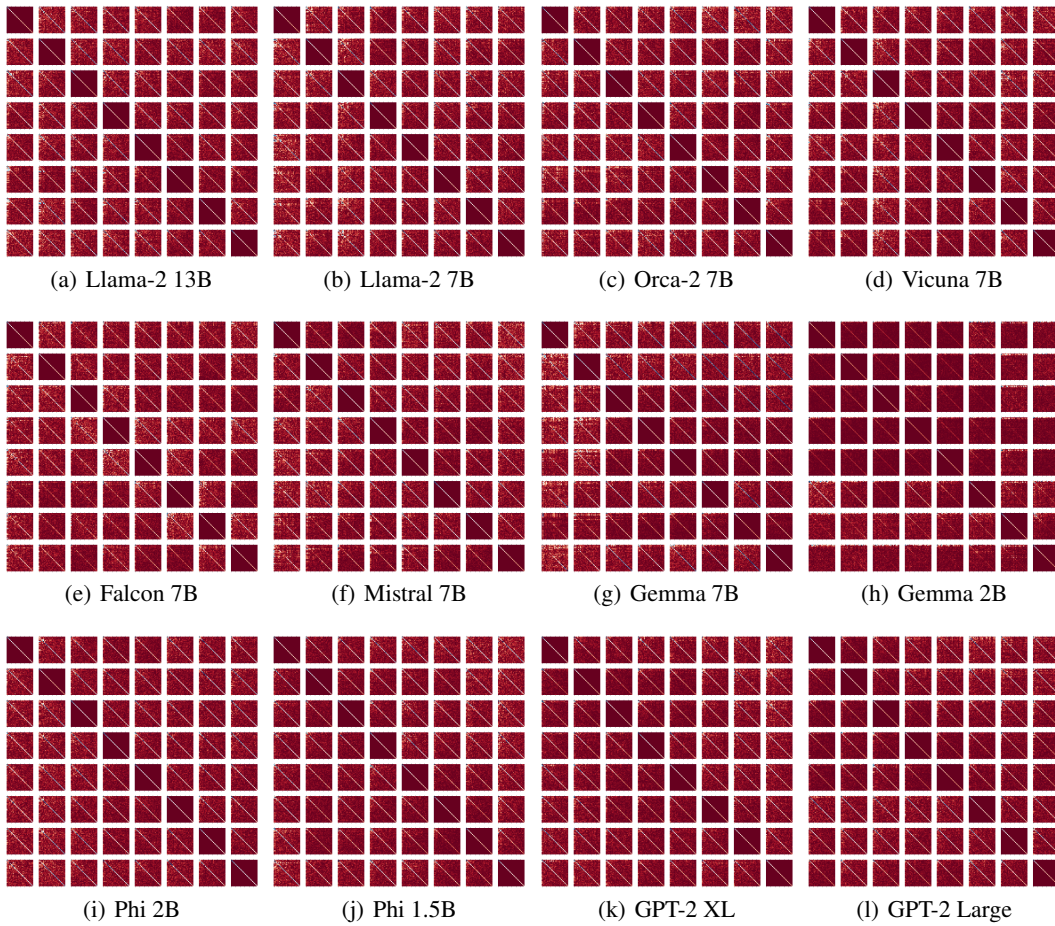


Figure 13: **Additional plots of Coupling across depth.** The figure illustrates the alignment of Residual Jacobians across transformer blocks 9 to 16.

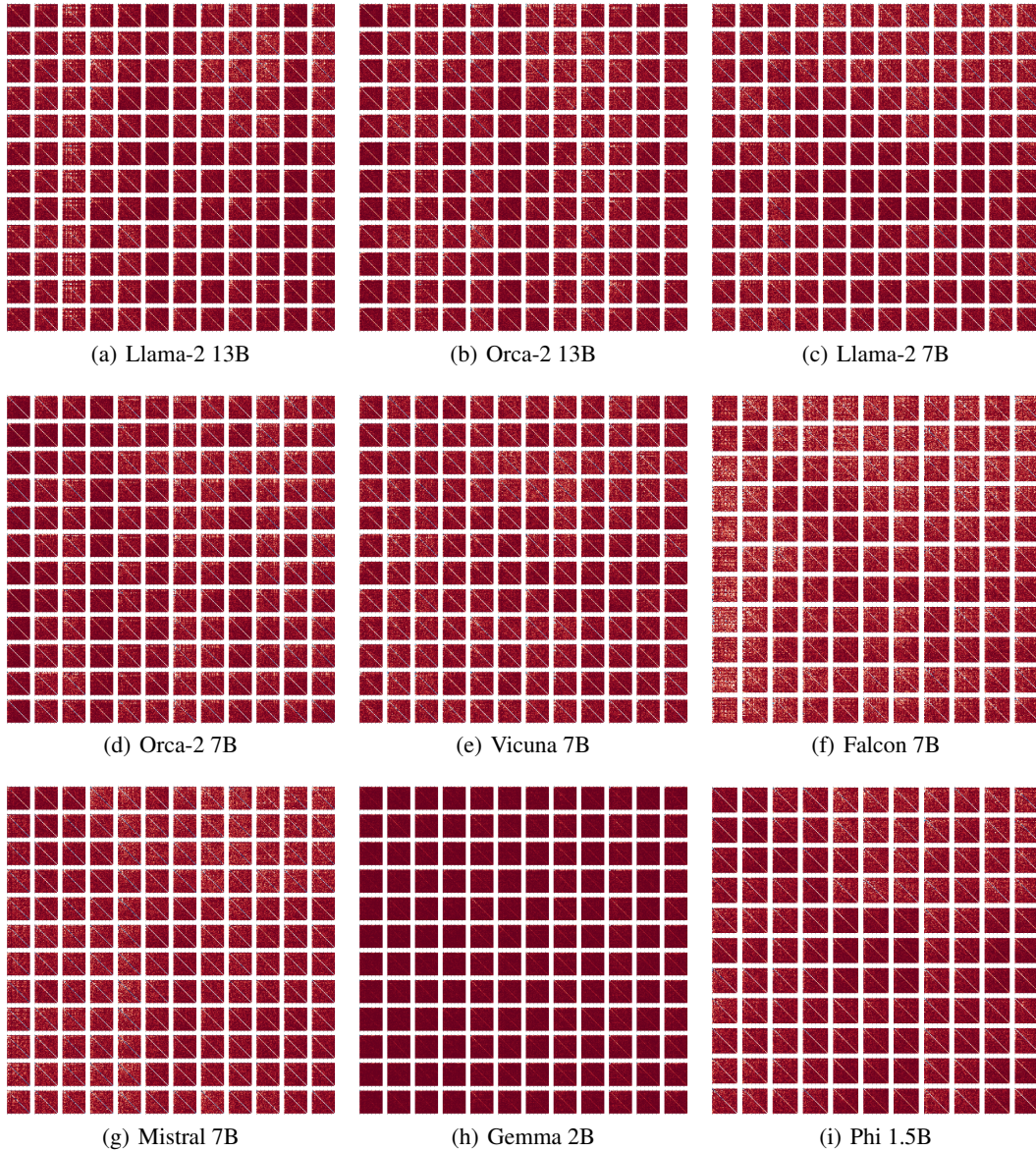


Figure 14: Additional plots of Coupling across Tokens (same input and output tokens).

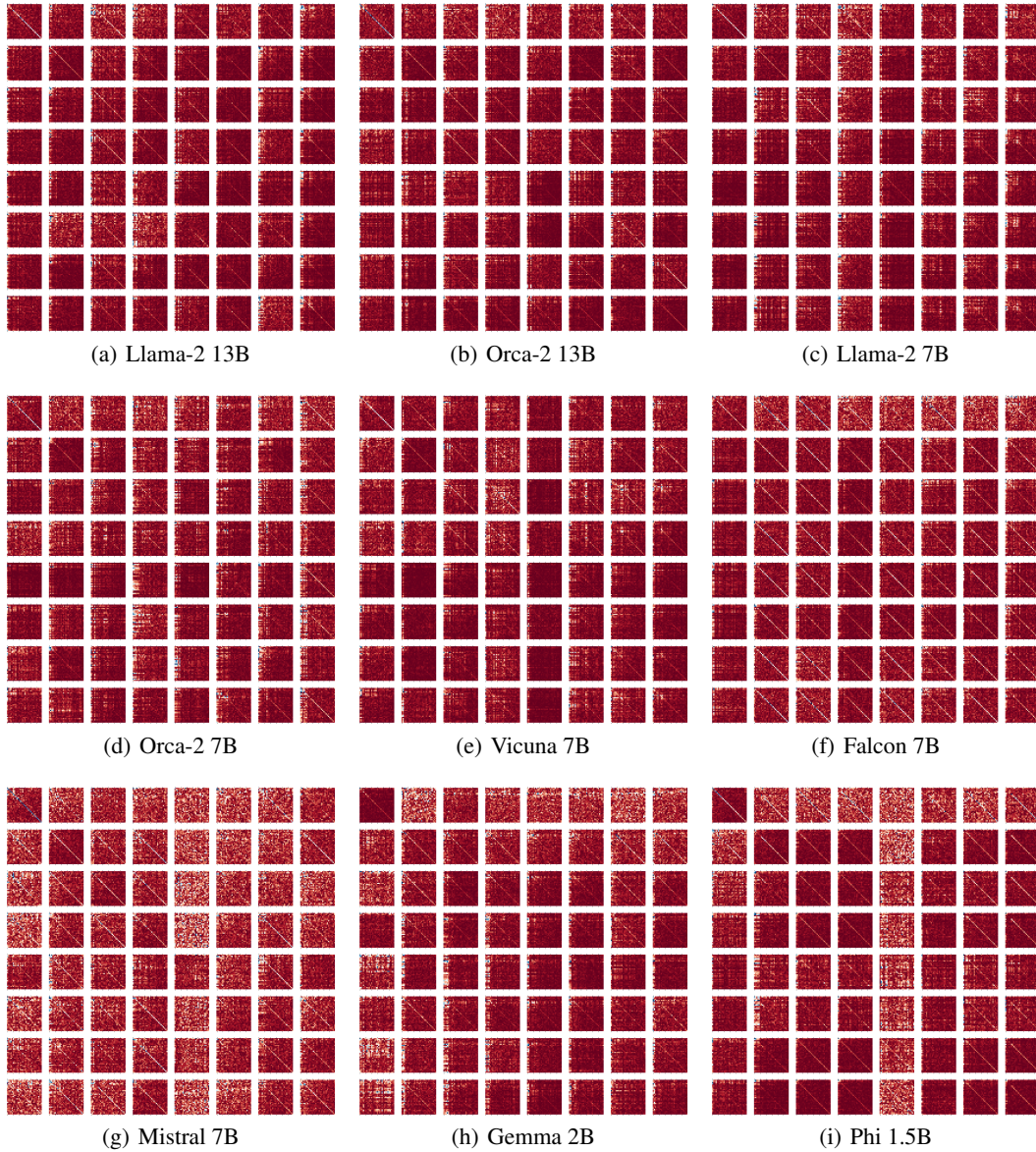


Figure 15: Additional plots of Coupling across Tokens (fixed input).

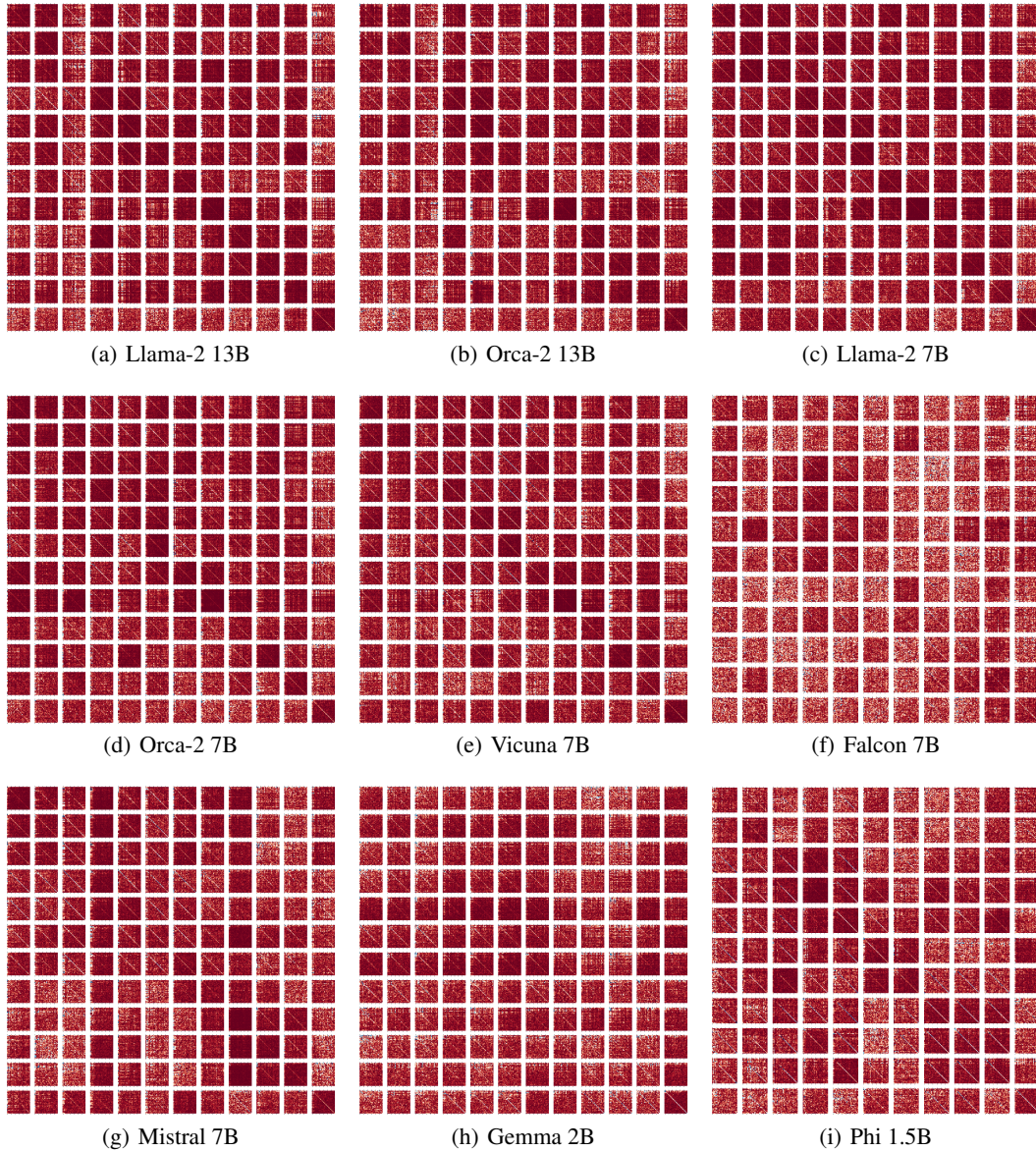


Figure 16: Additional plots of Coupling across Tokens (fixed output).

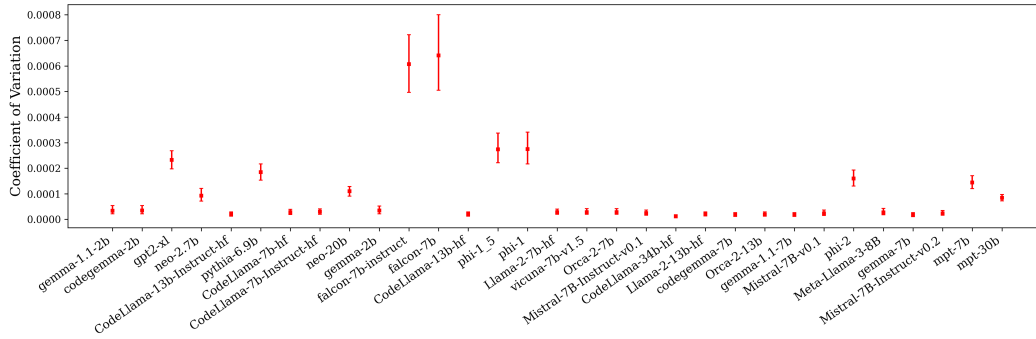


Figure 17: **Coefficient of variation of layer-wise equidistance.** Variation of layer-wise equidistance (Section 3.3) computed over 1,200 prompts from the HuggingFace Open LLM Leaderboard datasets (Section 4.2) on a suite of untrained LLMs (Appendix A.1). Plotted are the median values over all prompts, and are accompanied with uncertainty intervals depicting the inter-quartile range of the results for each model. The models are sorted by increasing benchmark performance.

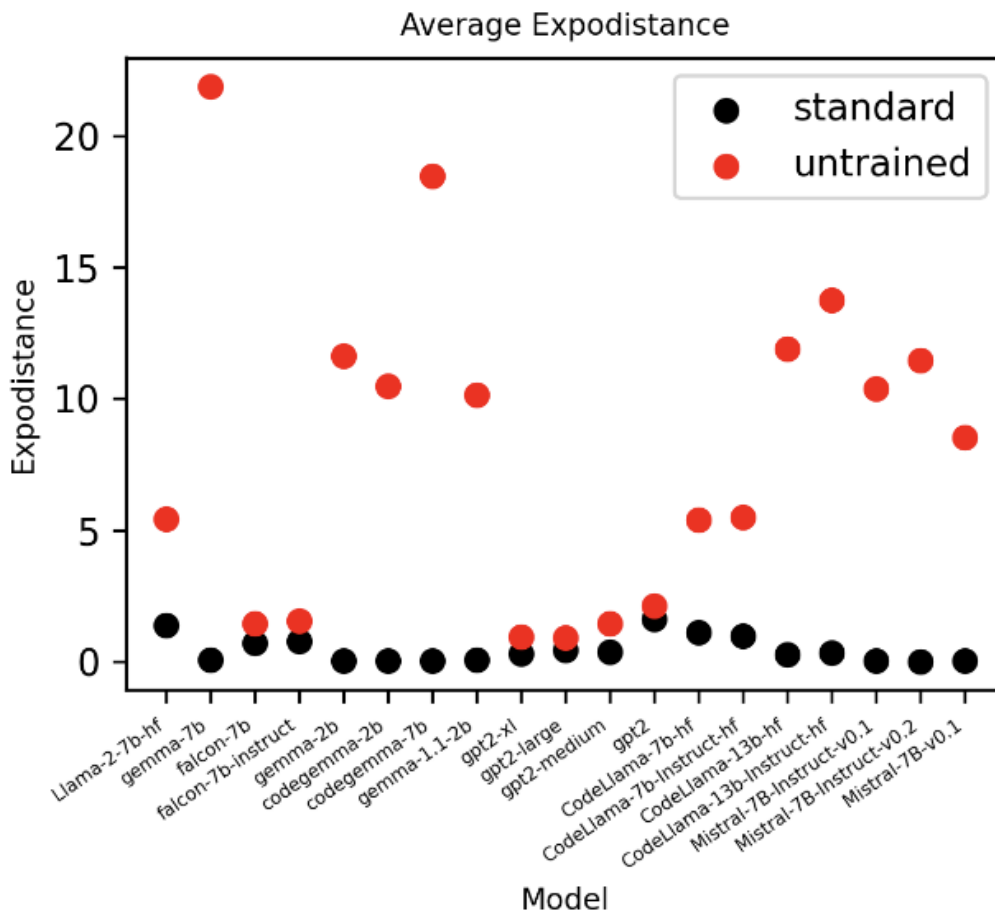


Figure 18: **Coefficient of variation of layer-wise expodistance.** Variation of layer-wise expodistance (Section 3.3) computed over 1,200 prompts from the HuggingFace Open LLM Leaderboard datasets (Section 4.2) on a suite of untrained LLMs (Appendix A.1).

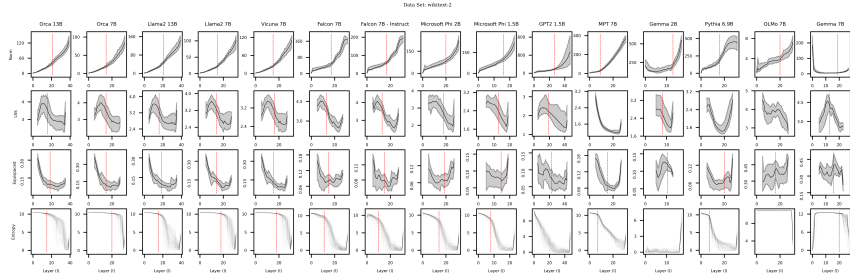


Figure 19: **Various Measurements of Representations.** All measurements were made on 100 prompts taken from the WikiText 2 datasets. **(Row 1)** Norm of hidden representations as a function of layer depth. **(Row 2)** Line Shape Score (LSS) of the hidden trajectories as a function of layer depth. **(Row 3)** Mean equidistance of contiguous hidden trajectories as a function of depth. **(Row 4)** Entropy of logit vectors as a function of depth. Noted in most plots is a line where the behaviour of the measurement drastically changes.

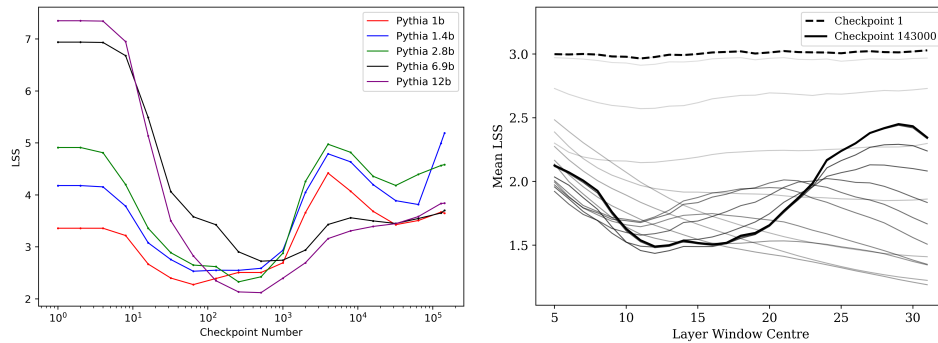


Figure 20: **Linearity Emerges with Training.** Two plots displaying the evolution of the linearity of the token trajectories through training. **(Left)** The LSS as a function of training checkpoint for the variants of the Pythia Scaling Suite Biderman et al. (2023). Here, the LSS is measured over each entire prompt. **(Right)** The mean LSS as a function of layer depth measured at various checkpoints throughout the Pythia 12B model. Here, the LSS is computed on a window of layers of width 11, centred at the value given by the x-axis.

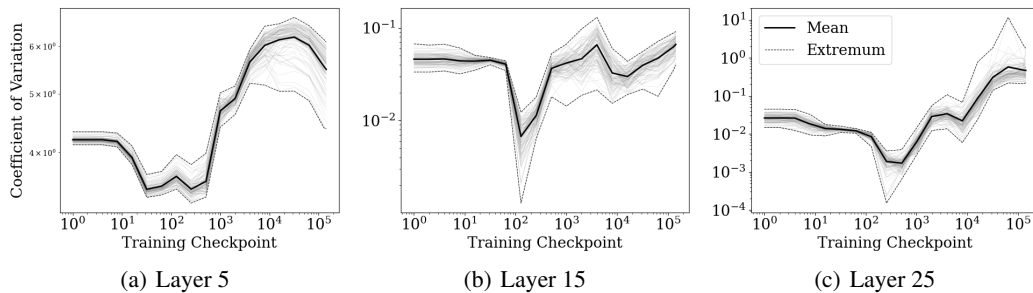


Figure 21: **Expodistance at Fixed Layers.** Plotted are mean expodistances as a function of training checkpoint at various depths of the network. The values at a given depth are the mean expodistance over a layer window of width 11 centred at said depth 100 MMLU prompts are plotted at each layer.

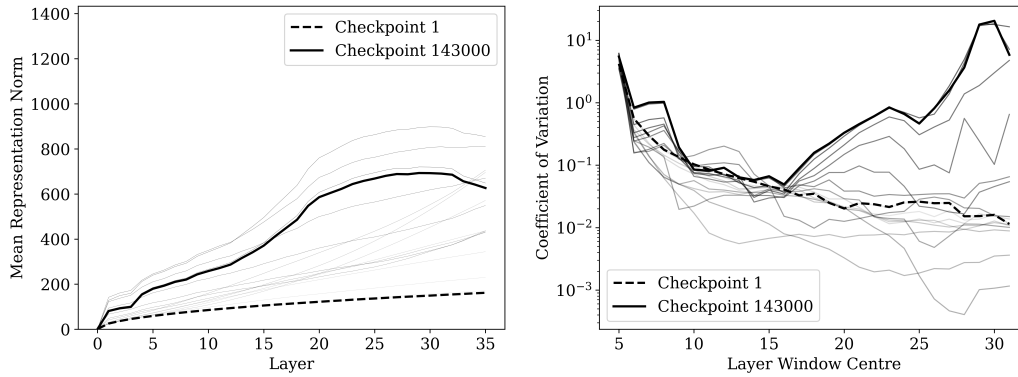
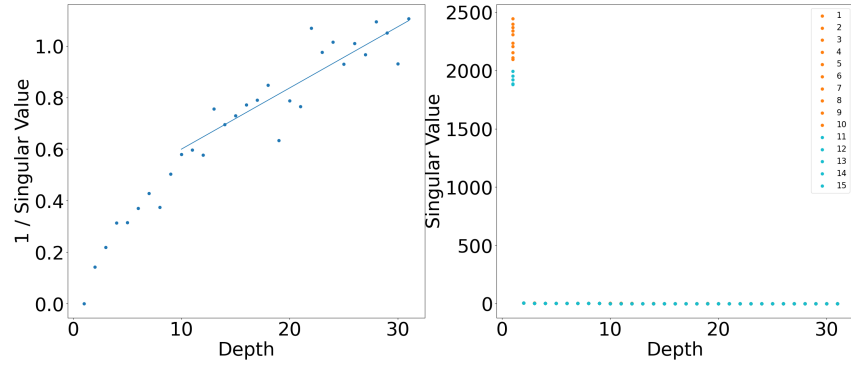
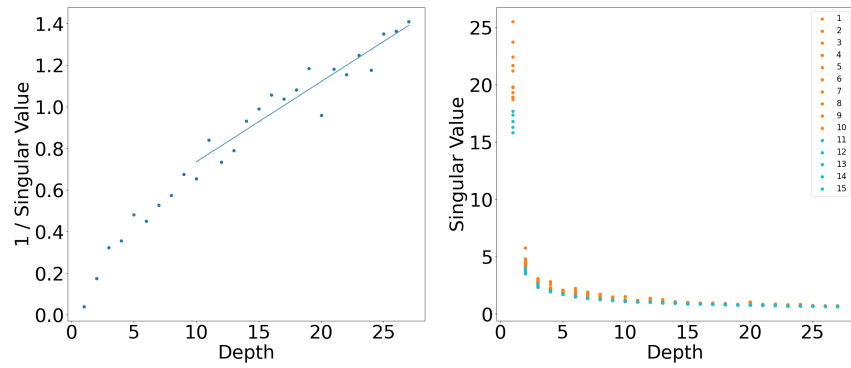


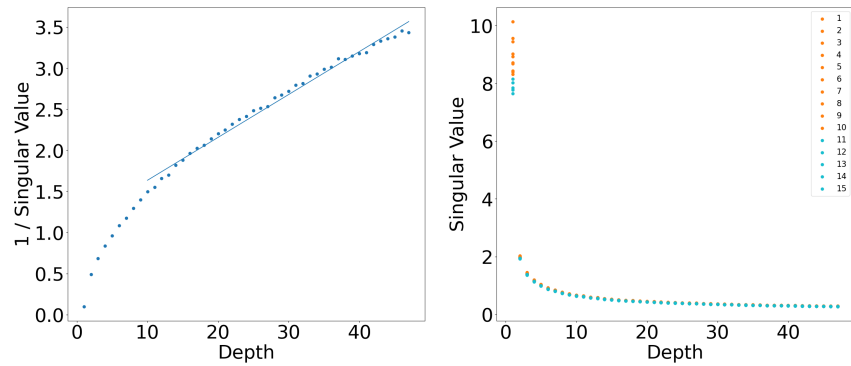
Figure 22: **Norm and Expodistance During Training.** (Left) Plotted is the norm of the representations as a function of depth at various training checkpoints. Observed is the transition from log-like growth in early stages to exponential-like growth, particularly through layers 5 through 20, as training evolves. (Right) Plotted is the expodistance over a layer window of width 11 centred at the given depth, each computed at a variety of training checkpoints.



(a) Llama-3 8B

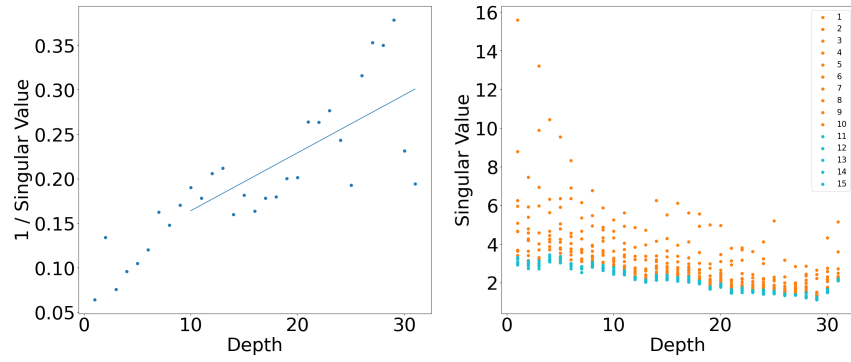


(b) Gemma 7B

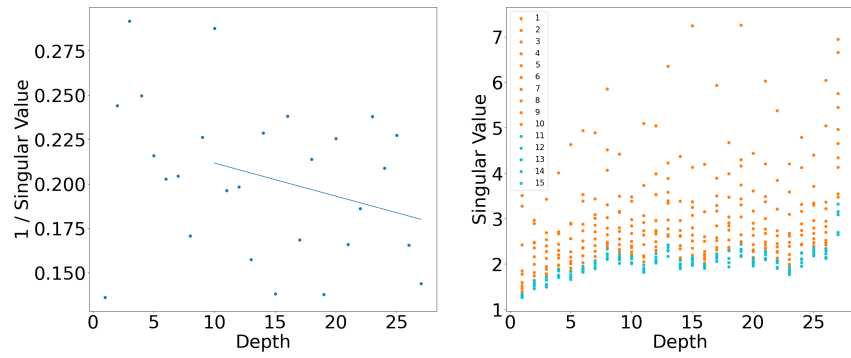


(c) GPT-2 XL

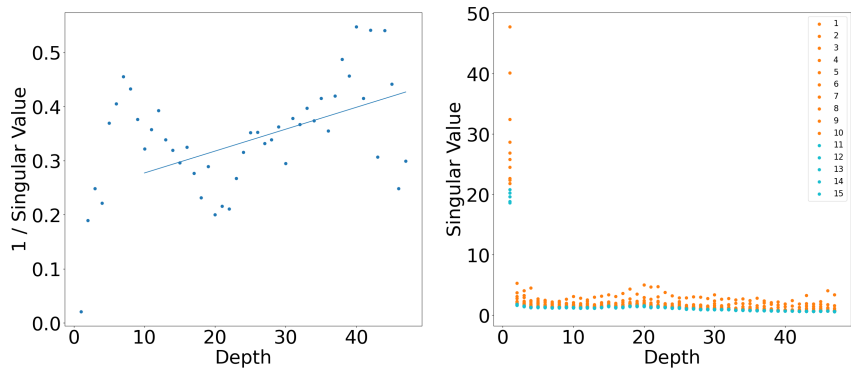
Figure 23: Scaling of Singular Values of Residual Jacobians (Untrained).



(a) Llama-3 8B

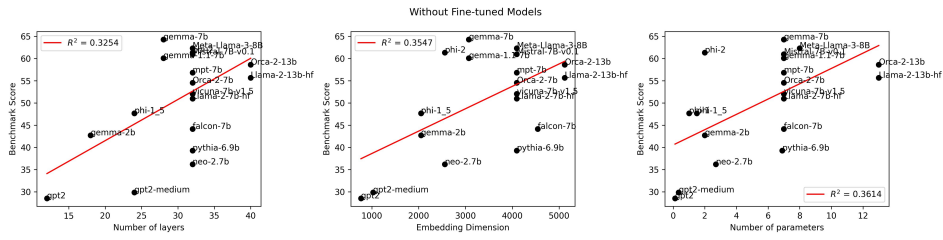


(b) Gemma 7B

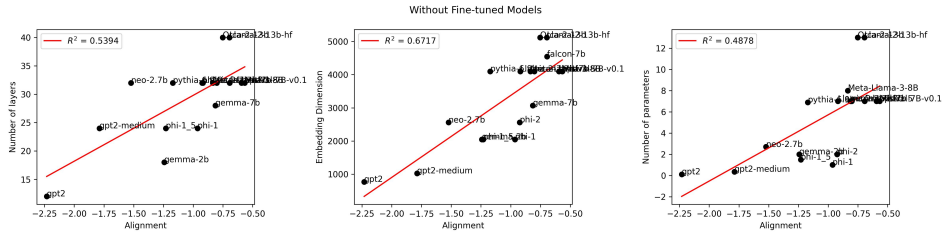


(c) GPT-2 XL

Figure 24: **Scaling of Singular Values of Residual Jacobians (Trained).**



(a) Score vs. hyperparameters



(b) Hyperparameters vs. Alignment

Figure 25: LLM number of layers, embedding dimension, and number of parameters, against score and Residual Jacobian Alignment.

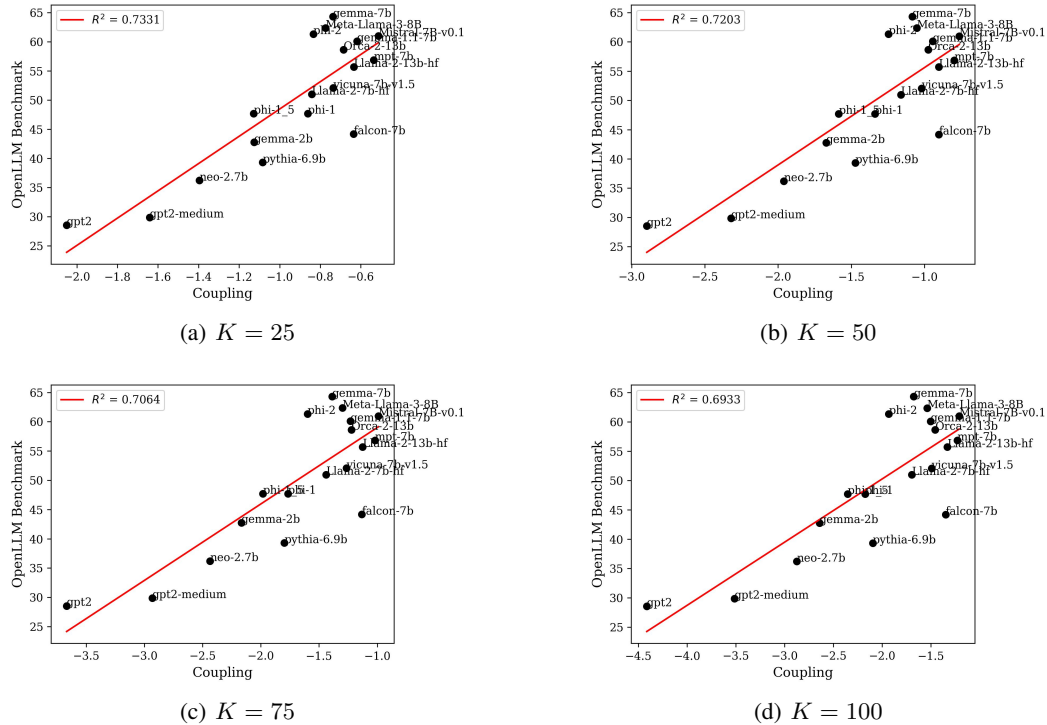


Figure 26: Coupling plotted against benchmark score for varying number of singular vectors.

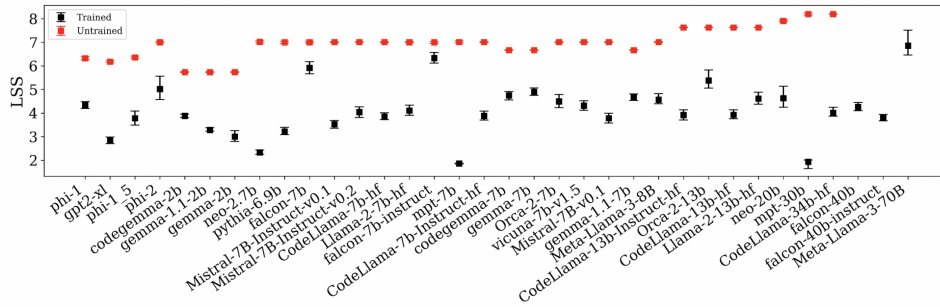


Figure 27: LSS sorted by LLM parameters.

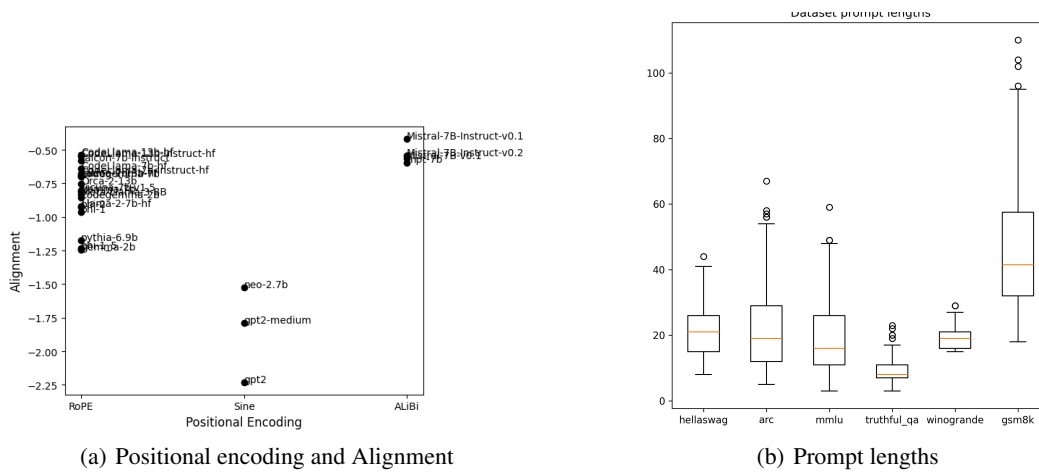


Figure 28: Other plots.

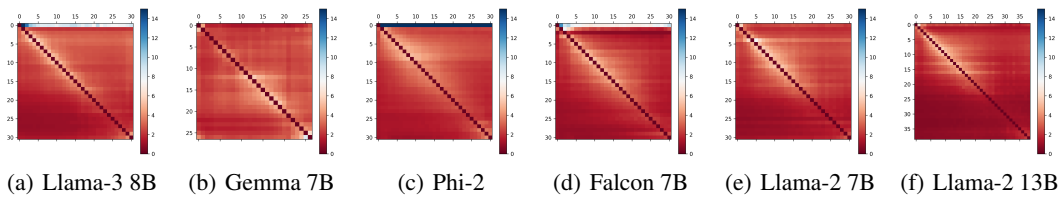


Figure 29: Layer-wise misalignment of Singular Vectors of Residual Jacobians.